Visualizing the dynamics of HIV-specific cytotoxic T-cells in extracellular matrix

By
Maria Hottelet Foley

B.S. Biology
Emory University, 1996

SUBMITTED TO DEPARTMENT OF BIOLOGICAL ENGINEERING
IN PARTIAL FULFILLMENT OF THE REQUIREMENTS FOR THE DEGREE OF

DOCTOR OF PHILOSOPHY
AT THE
MASSACHUSETTS INSTITUTE OF TECHNOLOGY
JUNE 2012

Signature of author:_____
Biological Engineering Department
February 27, 2012

Certified by:_____
Darrell J. Irvine
Associate Professor of DMSE and Biological Engineering
Thesis Supervisor

Accepted by:_____
Douglas A. Lauffenburger
Ford Professor of Biological Engineering, Chemical Engineering, and Biology
Chairman, Graduate Program Committee

Visualizing the dynamics of HIV-specific cytotoxic T-cells in extracellular matrix

by
Maria Hottelet Foley

Submitted to Department of Biological Engineering on February 27, 2012,
in Partial Fulfillment of the Requirements for the
Degree of Doctor of Philosophy in Biological Engineering

Cytotoxic lymphocytes (CTLs) traffic through tissues in search of antigen and mount protective immune responses against viral infections and cancer. While molecular mechanisms of CTL antiviral effector functions have been established *in vitro*, they have been defined in the absence of physiological dynamics and migration. Furthermore, long-term dynamics of single cells have been inaccessible *in vivo,* where brief imaging durations have been achieved (~30-60 min). Presently, several key aspects of CTL dynamics and function remain unknown: whether individual CTLs migrating within tissues kill multiple targets, if CTLs exhibit spatiotemporal coordination of effector functions, or if migrating CTLs effect these functions in different compartments. Thus, a mechanistic understanding of multidimensional CTL function might directly inform therapeutic strategies.

In this thesis, we first developed an approach for long-term high-speed optical imaging of cellular dynamics for continuous periods of 24 hours. HIV-specific CTLs were visualized as they encountered $CD4^+$ target cells within a three-dimensional extracellular matrix tissue model supporting migration of both CTLs and targets. Using this approach, we found that high-avidity CTLs engaged, arrested, and killed the first target encountered with near-perfect efficiency. These CTLs remained in contact with dead targets for hours, accumulating TCR signals and upregulating antiviral cytokine and chemokine secretion for ≥12 hours, but were refractory to killing additional targets. By contrast, lower-avidity CTLs exhibited poor efficiency and target migration directly impeded CTL killing. Thus, high-avidity CTLs coordinate multiple antiviral functions in four dimensions (3D space and time): effectively destroying the first detected infected cell during an initial "commitment phase", but rapidly transitioning to a prolonged "secretory phase." *In vivo,* coordination of lytic and non-lytic effector functions will direct the local inflammatory milieu and recruit additional effectors to the tissue. We conclude that the efficiency of antigen recognition by individual migrating CTLs is a critical, but previously undefined, parameter of CTL function. Furthermore, TCR avidity and initial CTL efficiency are prerequisites for sustained antiviral polyfunctionality; together these parameters define a highly effective, multidimensional CTL response, which may inform the design of increasingly effective vaccines.

Thesis Supervisor: Darrell J. Irvine

Title: Associate Professor of DMSE and Biological Engineering

TABLE OF CONTENTS

CHAPTER 1. INTRODUCTION AND BACKGROUND

1.1 INTRODUCTION AND SCOPE OF THESIS

Not only do cytotoxic T-lymphocytes (CTLs) play an important role in the adaptive cellular immune response to viral infections and cancer, but they can also inflict substantial autoimmune tissue damage and disease. CTLs possess a variety of lytic and non-lytic secretory functions which have been well-studied at the molecular level, but CTL activity has largely been defined in liquid suspension cultures *in vitro,* outside the relevant context of 3D tissue extracellular matrix which supports physiological motility. Although numerous CTL functions have been individually implicated in the control of infections and cancer (Almeida et al., 2009; Betts et al., 2006; Freel et al., 2010; Genesca et al., 2008; Mellman et al., 2011; Migueles et al., 2008; Uchida, 2011), the relationship between function and protection remains correlative. The important question of how migrating CTLs coordinate this array of functions within the 3D environment of tissue over time has remained unaddressed.

Effector $CD8^+$ cytotoxic T lymphocytes (CTLs) contribute to control of viral infections and cancer via target cell killing (mediated by perforin, granzyme, or FasL)(Ando et al., 1997; Asquith et al., 2005; Atkinson and Bleackley, 1995; Bangham and Osame, 2005; He et al., 2010; Keefe et al., 2005; Kojima et al., 2002; Thiery et al., 2011), and indirectly through the secretion of cytokines (such as interferon-γ or TNF-α) and β-chemokines (such as CCL3/MIP-1α, CCL4/ MIP-1β, or CCL5/RANTES) (Cocchi et al., 1995; Cocchi et al., 2000; DeVico and Gallo, 2004; Huse et al., 2008). These signaling molecules alter the inflammatory milieu of the infected tissue microenvironment, both recruiting additional leukocytes (Castellino et al., 2006) and promoting effector functions of nearby immune cells (Andrade, 2010; Guidotti and Chisari, 2001). In the

setting of HIV infection, it is well appreciated that β-chemokines directly block CCR5 chemokine receptor-mediated entry of the virus into nearby host cells (Cocchi et al., 1995; Scarlatti et al., 1997; Simmons et al., 2000; Yang et al., 1997), and high capacity for β-chemokine production correlates inversely with viral load (Cocchi et al., 2000; Dolan et al., 2007; Ferbas et al., 2000; Kulkarni et al., 2008). However, there have been no studies directly examining the functional effect of β-chemokines produced by CTLs *in vivo*.

Given the importance of CTLs in the immune response to viruses and cancer, there is a great need for quantitative *in vitro* assays of CTL function delivering predictive, rather than correlative, measures of protective CTL function *in vivo.* To address this need, in this thesis we developed a new approach for long-term high-speed dynamic optical imaging to visualize the dynamic interactions of migrating human HIV-specific CTLs and target cells, with resolution at the single-cell level. Importantly, CTL effector functions were visualized, measured, and perturb ed within an extracellular matrix model of tissue, where both CTLs and target cells are highly motile with dynamics resembling those observed *in vivo.* The interactions of CTLs and targets have been tracked for up to 24 hrs continuously, permitting analysis of CTL-target engagement dynamics (both short and long-term) and CTL functions (including those with rapid and delayed kinetics). This approach allowed us to examine prolonged CTL-target interactions that cannot be observed and manipulated with current methods *in vivo*. We also introduce an integrated model of protective, multidimensional CTL function that could be used to guide the development of cell-mediated vaccines for HIV, other viruses, or cancer.

1.2 BACKGROUND

1.2.1 Mechanisms of CTL killing

There are at least several molecular mechanisms by which CTLs induce target cell death, but their functional roles *in vivo* are just beginning to be understood (Janssen et al., 2010; Meiraz et al., 2009). These mechanisms include FasL mediated apoptosis, perforin and granzyme mediated apoptosis with transient membrane permeabilization, and complete, rapid perforin-mediated lysis of the target cell membrane (He et al., 2010; Keefe et al., 2005; Lowin et al., 1994; Thiery et al., 2011; Waterhouse et al., 2006). Each of these lethal hits induces morphologically distinct changes in the dying target cell (Keefe et al., 2005; Waterhouse et al., 2006) and each of these mechanisms are preferentially induced with unique thresholds of antigen recognition, from most sensitive: FasL > perforin and granzyme > perforin-mediated lysis (Esser et al., 1996; He et al., 2010; Keefe et al., 2005). Interestingly, CTLs may utilize these mechanisms of killing in combination since it is reported that FasL is found within the same secretory vesicles as granzymes (Zuccato et al., 2007).

1.2.2 Molecular mechanisms and kinetics of CTL effector function

CTL functions have been largely characterized outside the three-dimensional ECM context of tissues in liquid suspensions where cells encounter each other as a result of convection. In this setting, in the absence of physiological migration, CTL contact with a target cell is accompanied by a prototypical series of events (**Figure 1.1**): TCR recognition of cognate peptide-MHC-I on the target cell, calcium signaling coincident with a TCR-dependent stop signal (within seconds) (Huse et al., 2007; Purbhoo et al., 2001; Stinchcombe et al., 2001), motility arrest, and cytoskeletal polarization towards the target cell (seconds to minutes) (Dustin et al., 1997), signs of target death including membrane blebbing (2-20 minutes) (Matter, 1979; Stinchcombe et al., 2001), and target cell permeabilization (~3 hours) (Jenkins et al., 2009a). Secretion of non-lytic,

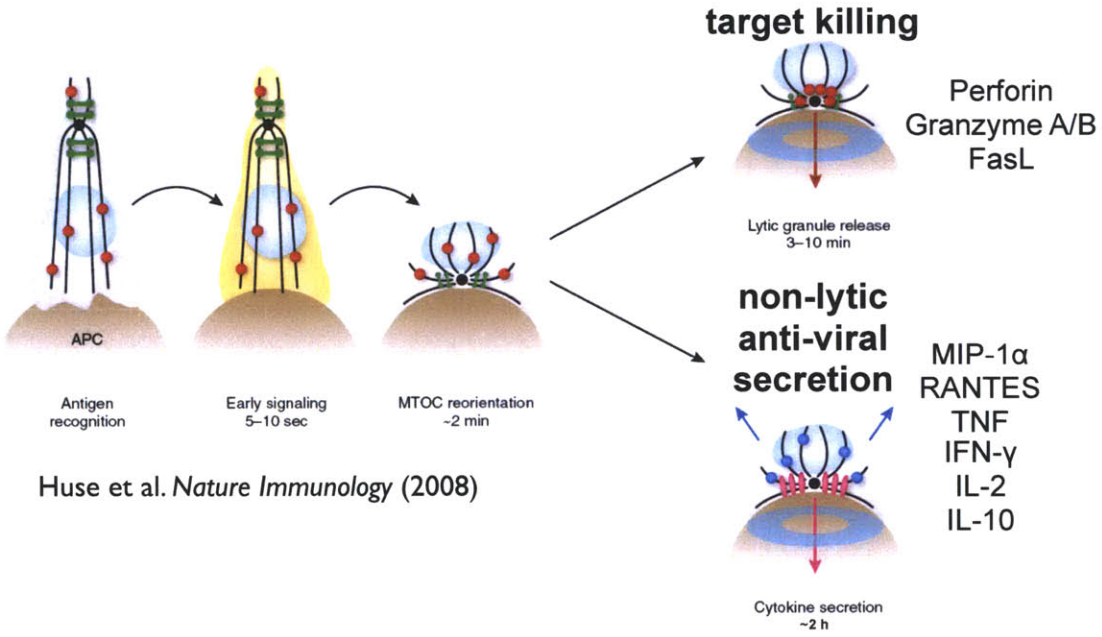

Figure 1.1: Schematic of molecular mechanisms of CTL function adapted from (Huse et al., 2008)

anti-viral factors including cytokines (IFN-γ, IL-2, TNF, IL-10) and chemokines (CCL3, CCL4, CCL5) is TCR-dependent **(Figure 1.2)** (Catalfamo et al., 2004; Faroudi et al., 2003; Valitutti et al., 2010; Valitutti et al., 1996). Interestingly, CTL function can be described in two phases with

different requirements for activation: lethal hit delivery (the early phase) is highly sensitive to antigen, while cytokine/chemokine secretion and proliferation (the later phase) requires much stronger TCR signals supporting gene transcription. Thus, target killing and full effector function are uncoupled in the absence of strong TCR signals (Faroudi et al., 2003; Porgador et al., 1997; Valitutti et al., 1996; Wiedemann et al., 2006).

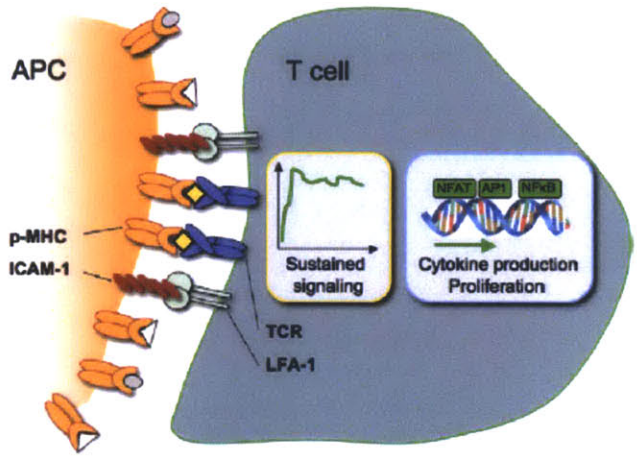

Figure 1.2: Strong TCR signaling results in coordination of CTL functions with low and high thresholds of antigen sensitivity (Valitutti et al., 2010).
Weak signaling results in uncoupling of CTL functions based on differing thresholds of antigen sensitivity. CTL killing is an exquisitely sensitive response, while full effector function requires strong TCR signals. CTL (T cell) engagement of the target cell (APC) occurs upon TCR recognition of cognate peptide-MHC-I on the target. Cell-cell membrane apposition is accomplished through receptor-ligand binding of various pairs of integrins and adhesion molecules including LFA-1 and ICAM-1, respectively.

Early, pioneering time-lapse microscopy studies that reported CTLs occasionally killed multiple targets targets (**Figure 1.3**) (Cerottini and Brunner, 1974; Isaaz et al., 1995; Martz, 1976; Matter, 1979; Poenie et al., 1987; Rothstein et al., 1978; Zagury et al., 1975) and based on small numbers of CTL killing events, led to the notion of CTL "serial killing". While this mechanism has persisted conceptually for almost 40 years, serial CTL killing has yet to be observed in the context of cell migration *in vitro* or *in vivo*, and the physiological relevance of this mechanism remains unconfirmed. In addition, it remains unclear whether migrating CTLs accumulate enough TCR signal for full effector function through one prolonged engagement or short, serial engagements with targets (**Figure 1.4**).

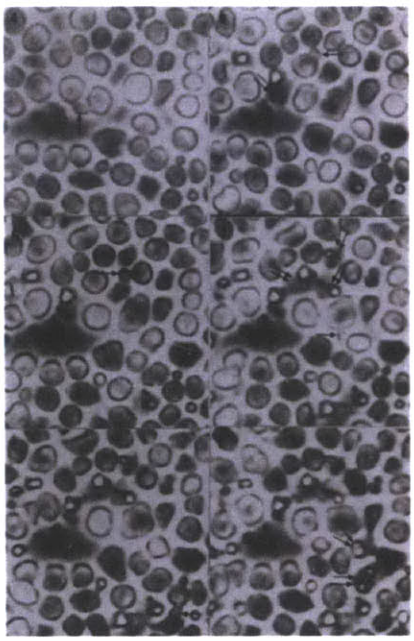

Figure 1.3: Pioneering timelapse "microcinematography" of CTL killing in liquid suspension (Rothstein et al., 1978).
Early microscopy studies observed CTLs killing targets in brightfield. Cell morphology was used to distinguish CTLs from target cells and live cells from dead cells. (**a**) A series of images of an individual mouse tumor-specific CTL (indicated by single arrows) interacting with target cells. 15 targets are contacted by the CTL over 410 minutes. 6 targets died during the course of imaging (indicated with double arrows). One example of 4 individual CTL examined is shown.

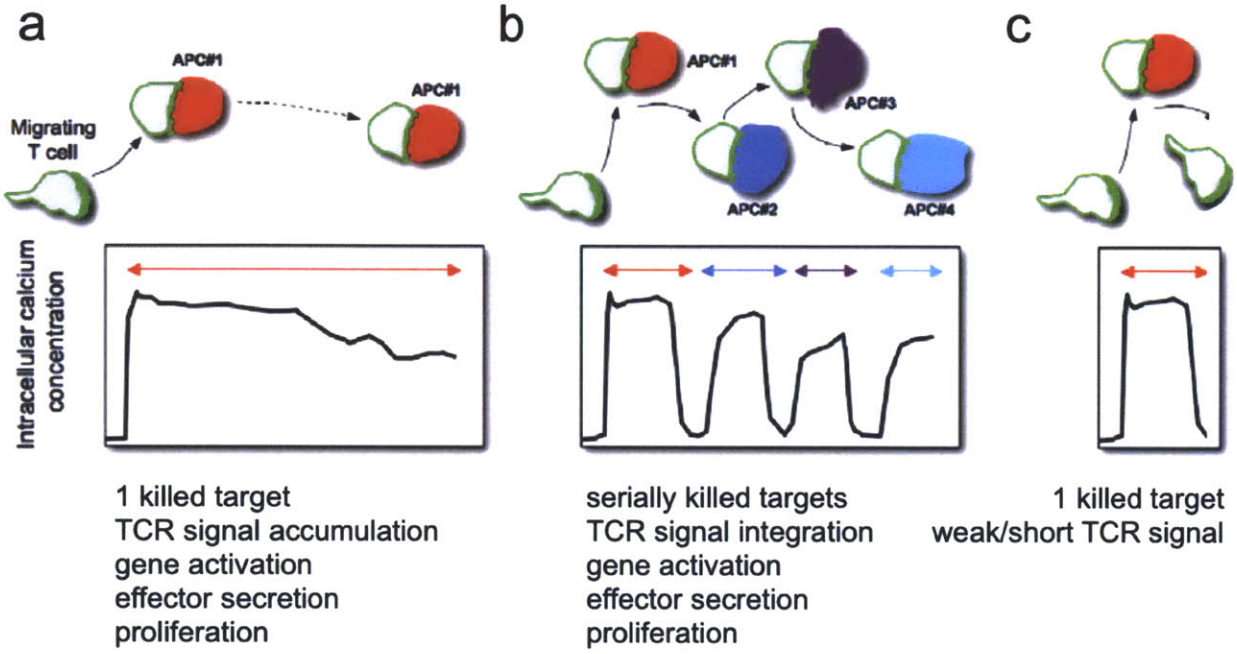

Figure 1.4: Schematic of potential CTL-target encounter dynamics and their effects on CTL effector function. Figure adapted from (Valitutti et al., 2010).

Migrating CTLs engage and kill targets in response to weak TCR signaling, but may continue to acquire additional strong or weak TCR signals depending on the length of CTL-target engagement. Strong TCR signals are required for full gene activation, effector function and proliferation. (**a**) A CTL acquires strong, prolonged TCR signals upon killing one target. (**b**) If an individual CTL serially kills multiple targets over time, it might successfully acquire and integrate enough signal to achieve partial or full effector function. (**c**) Killing is uncoupled from full effector function for an individual CTL killing a single target as the result of less total integrated TCR signaling.

1.2.3 CTL dynamics and function in vivo

Intravital and whole-organ *ex vivo* imaging studies in mice have revealed that T-cells execute a random walk-like search for antigen (**Figure 1.5**) but undergo TCR-triggered motility arrest upon engaging an antigen-bearing cell (Miller et al., 2002; Stoll et al., 2002). Visualization of individual CTLs *in vivo* in mice has revealed rapid lethal hit delivery kinetics (Breart et al., 2008; Mempel et al., 2006), and late periods of CTL arrest in the presence of antigen (Boissonnas et al., 2007; Deguine et al., 2010; Mrass et al., 2006), associated with slow rates of CTL killing (Breart et al., 2008; Coppieters et al., 2011). However, imaging durations achieved *in vivo* (currently lasting ~30 minutes) have thus far precluded single-cell analysis of long-term CTL motility dynamics, and observation of CTL killing and kinetics of target death *in vivo* is restricted by the need for the fluorescence reporting of these events. Thus far, only three reports have achieved *in vivo* visualization of CTL migration dynamics and the effects of CTL engagement on target viability: these studies have relied on two-photon imaging and sophisticated fluorescence strategies measuring ratiometric changes in the fluorescence of two reporters (small molecule or genetic) to assess target death and a third fluorescence marker to visualize CTLs (Breart et al., 2008; Coppieters et al., 2011; Mempel et al., 2006). Thus, current limitations on *in vivo* imaging strategies preclude continuous single-cell visualization of all phases of CTL effector response: initial TCR triggering, CTL arrest, and target death which occur with rapid kinetics, and secretion of effector cytokines/chemokine which depend on the slower processes of TCR signal integration and gene activation.

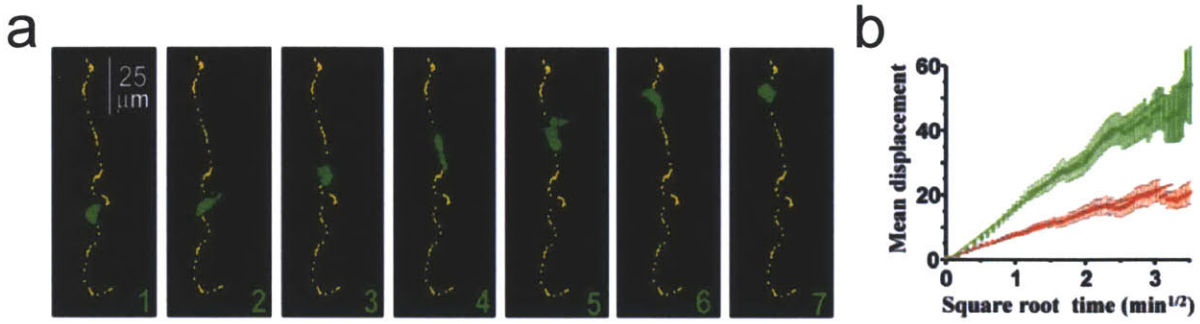

Figure 1.5: T cell lymphocyte migration within lymph node explants
T cells are highly motile and exhibit a random-walk in search of antigen within tissue. (**a**) An individual T cell exhibits migration. (**b**) Quantitative analysis of migration dynamics for T cells (green) and B cells (red) indicating random-walk behavior (Miller et al., 2002).

1.2.4 The role of HIV-specific CTLs in viral suppression in HIV-infected patients

It is estimated that 1 in 300 patients infected with HIV spontaneously control infection, and these "elite controllers" or "non-progressors" maintain low or undetectable levels of virus in the blood delaying progression to AIDS for years and sometimes decades (Baker et al., 2009). These patients have been intensely studied with the hope that their immune systems hold the key to a vaccine or cure for HIV. Although many immunological mechanisms have been found to correlate with control of HIV *in vivo*, a mounting body of evidence supports a key role for HIV-specific CTLs in HIV-infected patients who control the virus (Baker et al., 2009; Betts and Harari, 2008; McMichael et al., 2010; Poropatich and Sullivan, 2011). CTLs purified from elite controllers are capable of suppressing viral replication in liquid suspensions *in vitro* independent of other immune cells or factors (**Figure 1.6**) (Fauce et al., 2007; Freel et al., 2010; Julg et al., 2010; Saez-Cirion et al., 2007; Saez-Cirion et al., 2010). *In vivo*, CTL depletion results in increased viral loads in non-human primate models (Friedrich et al., 2007; Schmitz et al., 2005; Schmitz et al., 1999), and there are inverse correlations of viral load with metrics of CTL function such as antigen sensitivity (Almeida et al., 2007; Almeida et al., 2009; Bennett et al., 2007), CTL expression of β-chemokines (Cocchi et al., 2000; Dolan et al., 2007; Ferbas et al., 2000), lytic capacity (Hersperger et al., 2010; Migueles et al., 2002; Migueles et al., 2008), Gag-specific CTL responses (Julg et al., 2010; Kiepiela et al., 2007), CTL polyfunctionality (Almeida et al., 2007; Almeida et al., 2009; Betts et al., 2006; Freel et al., 2010), and proliferation (Betts et al., 2006; Migueles et al., 2002) in HIV^+ individuals. Such findings have motivated the development of vaccines aiming to elicit strong $CD8^+$ T-cell responses, and recent studies have shown in non-human primate models that robust CTL responses can lower setpoint viral load (Barouch et al., 2010) or even control virus to undetectable levels over time (Hansen et al., 2011;

Hansen et al., 2009; Liu et al., 2009; Tjernlund et al., 2010). Efforts to understand CTL-mediated mechanisms of viral suppression indicate that both lytic activity and cytokine/chemokine secretion can inhibit viral replication in $CD4^+$ target cells *in vitro* (Fauce et al., 2007; Yang et al., 1997). While the characteristics of CTLs that control HIV *in vivo* remain correlative, they indicate that multiple dimensions of CTL activity are important in viral suppression. An integrated understanding of these CTL activities would provide a stronger model of effective CTL function. Such a model would likely inform the design of enhanced vaccine candidates.

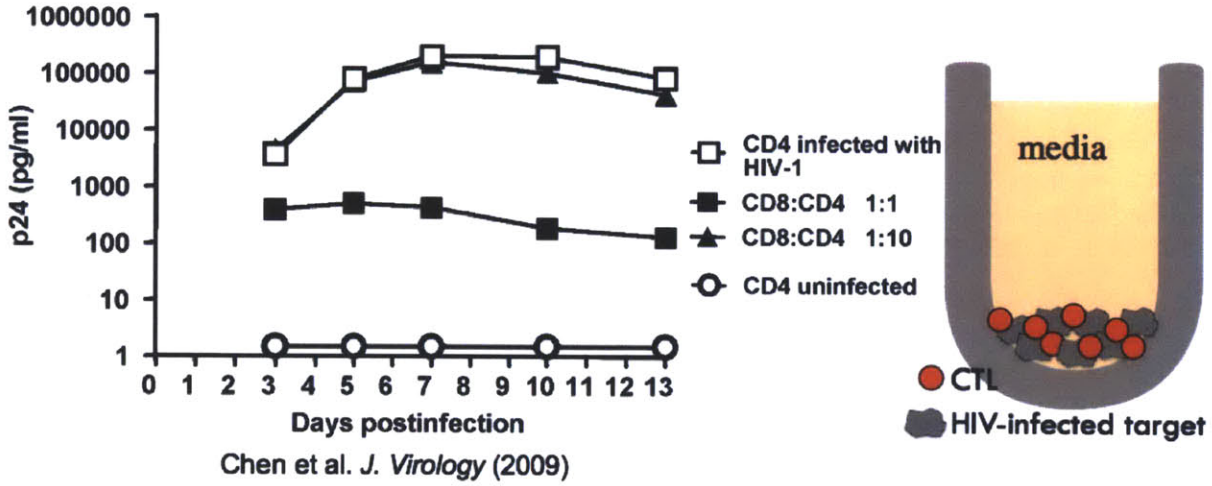

Figure 1.6: Primary HIV-specific CTLs suppress replication of HIV in vitro (Chen et al., 2009)

CTLs taken from elite controllers, patients who spontaneously control virus *in vivo*, exhibit anti-viral activity in liquid co-culture with autologous $CD4^+$ T cells infected with HIV.

1.2.5 The role of lymphocyte motility in HIV infection

Cytotoxic T-lymphocytes (CTLs) circulate through blood and actively migrate through three-dimensional tissue compartments in search of antigen in the periphery (Kawakami et al., 2005) and lymph nodes (Mempel et al., 2006; Miller et al., 2004; Miller et al., 2002). Notably, infected $CD4^+$ cells are motile (Nobile et al., 2010) and these infected $CD4^+$ cells contribute to the dissemination of virus from the local site of initial infection to distal tissues *in vivo* (Haase, 2010; Li et al., 2009a; Zhang et al., 1999). Thus, CTLs must catch migrating infected targets within various tissues including the lamina propria of the reproductive tract, gastrointestinal tissues, and within lymphoid organs (**Figure 1.7**) (Hong et al., 2009; Li et al., 2009a; Li et al., 2009b; Tjernlund et al., 2010). While HIV-specific CTLs exhibit markers of lytic and non-lytic effector functions within the extracellular matrix (ECM) of sectioned tissue (Genesca et al., 2008), it is not clear if they acquire sufficient TCR signals to drive non-lytic effector function through serial or prolonged contact with targets.

Following vaccination CTLs are detected in mucosal tissues prior to viral challenge (Belyakov et al., 2006; Hansen et al., 2011; Kaufman et al., 2009) and contribute to vaccine-induced viral control in non-human primates (Freel et al., 2010; Genesca et al., 2008). In the absence of prophylactic vaccination, CTL effectors typically arrive in the mucosal tissues too late to contain nascent viral infection (Reynolds et al., 2005). Thus, vaccine-induced establishment of resident HIV-specific CTLs in mucosal tissues likely contributes to the efficacy of these vaccines.

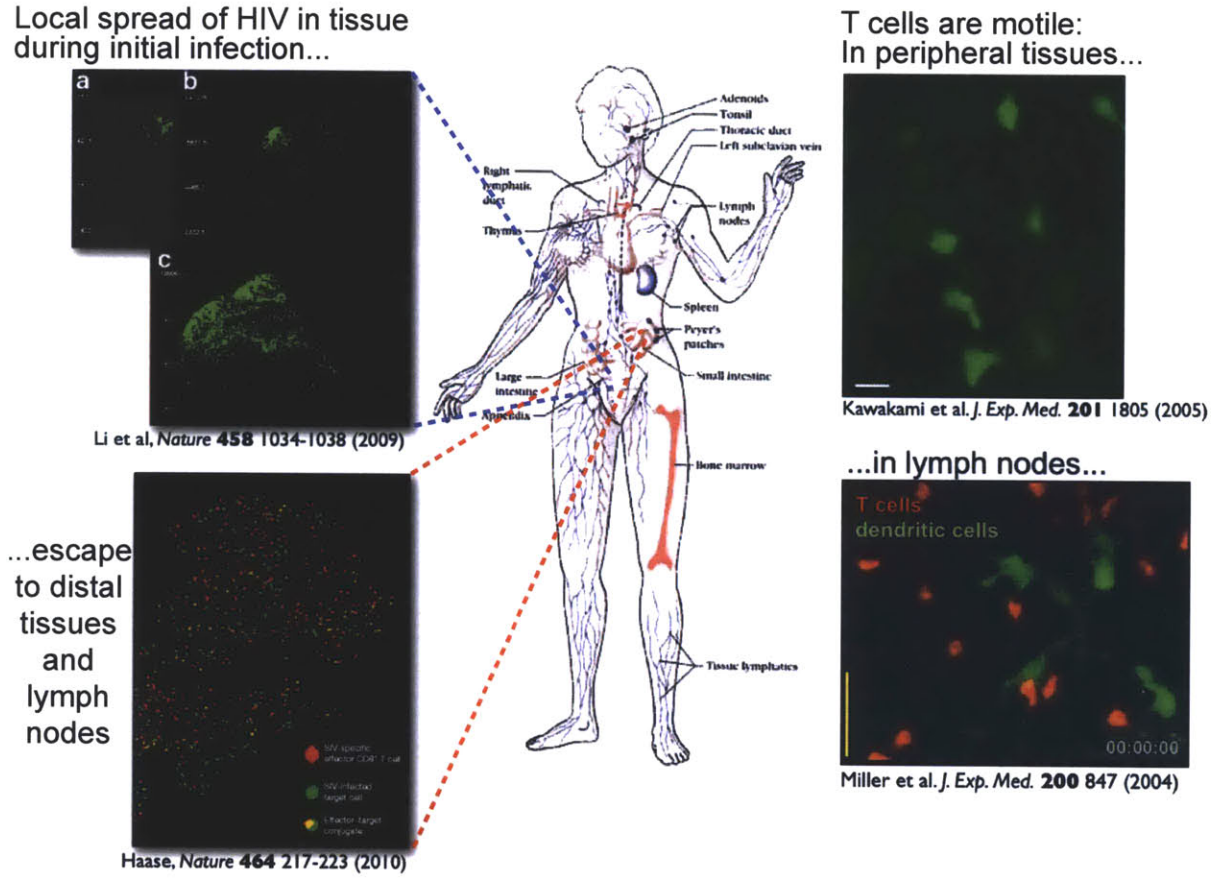

Figure 1.7: Lymphocyte motility plays an important role in the spread or containment of HIV *in vivo*.

1.3 AIMS AND SCOPE OF THESIS

In this thesis, we have applied quantitative analyses and a new high-speed strategy for time-lapse fluorescence imaging to study cell migration and engagement dynamics over time. We have specifically focused on the interactions between two populations of immune cells, examining the function of cytotoxic lymphocytes as they engage and kill antigen-bearing $CD4^+$ target cells. We have chosen a suitable reductionist extracellular matrix model of three-dimensional tissue to support lymphocyte-intrinsic cellular migration dynamics. We have focused specifically on HIV-specific CTL function, choosing to examine two human CTL clones and primary CTLs from one healthy HIV^+ person with a strong immune response to HIV. These CTLs were co-cultured with primary human $CD4^+$ T cells as model targets. We have chosen synthetic peptides as model antigens for presentation by these targets, modulating the CTLs sensitivity to antigen by varying either antigen density on the target or by varying peptide sequence thus controlling CTL functional avidity. HIV-infected $CD4^+$ T cells were included as more physiologically relevant targets in support of the studies of peptide-pulsed model targets. With this model system we have analyzed the single-cell dynamics of CTL-target engagement, the efficiency of individual CTL killing, and the coordination of killing with development of full effector secretory function over time.

Aim 1: Development of a video-microscopy assay for direct observation of motile CTL killing

We designed a strategy for the acquisition of internally-controlled video-microscopy data sets. This strategy utilized a high-speed motorized stage to collect serial images from four samples at a time, with at least one control sample in every imaging run. We identified a new combination of commercially available fluorescence markers for the *in situ* differentiation of

CTLs from $CD4^+$ T-cells and live cells from dead cells during long-term time-lapse microscopy. Cellular dynamics were visualized within a three-dimensional fibrillar collagen gel model of peripheral tissue supporting lymphocyte migration mimicking the dynamics reported *in vivo*. We evaluated and confirmed CTL lytic function within collagen gels using traditional ^{51}Cr release assays. Control experiments confirmed maintenance of cell viability during imaging and detection of antigen-dependent target death. Motile CTLs and targets were imaged in the absence of antigen and quantitative analyses of these antigen-independent engagement dynamics established a solid framework from which we could begin to examine antigen-dependent CTL engagements, killing and function in Aim 2.

Aim 2: Characterization of HIV-specific CTL function within a 3D extracellular matrix model of peripheral tissue

Migrating HIV-specific CTLs were directly visualized as they encountered either peptide-pulsed or HIV-infected primary human $CD4^+$ target cells. We identified 4 characteristic types of CTL-target engagements and established metrics to quantitatively describe the complex antigen-dependent behaviors and outcomes. These metrics included dose-dependent changes in CTL-target cell engagement frequencies, kinetics of TCR signaling and CTL arrest, engagement durations, target death kinetics, efficiency of CTL target killing during the first target encounter and all subsequent target encounters, the durability of CTL arrest over time, and the total number of targets killed by or escaped from each individual CTL. This work revealed two diametric perspectives on CTL-target engagement dynamics, of particular interest in the case of HIV where the success or failure of each discrete engagement may contribute to either containment of nascent infection by successful CTLs or systemic spread of virus by escaping targets. The CTL-

centric view captured changes in CTL migration/arrest and CTL killing efficiency following an initial kill; and indicated a correlation between TCR signaling strength/duration and CTL success or failure. The target-centric view suggested that target motility contributes directly to target escape from inefficient CTL engagements marked by weak TCR signaling. These correlations inspired the perturbations included in Aim 3.

Aim 3: Probe the effects of CTL antigen-sensitivity and target motility on CTL killing efficiency

Having developed a rich and multi-faceted picture of antigen-dependent CTL-target engagement dynamics, CTL killing, and CTL arrest as functions of antigen dose and time, the goal of Aim 3 was to perturb the system. First, we exploited a panel of peptide variants, recognized by one CTL clone with varied functional avidity, to examine the effects of antigen-sensitivity on the single-cell efficiency of CTLs. Next, we designed a strategy to immobilize $CD4^+$ target probing the effect of target mobility/immobility on target susceptibility to killing.

CHAPTER 2. MATERIALS, METHODS AND INSTRUMENTS

2.1 BASIC CELL CULTURE AND REAGENTS

2.1.1 Patient Samples

Peripheral blood mononuclear cells were obtained from healthy donors through Research Blood Components, Cambridge, MA and from HIV-infected persons through the outpatient clinics at Massachusetts General Hospital, Brigham and Women's Hospital, and Fenway Health in Boston, MA. Studies were approved by the MGH and MIT institutional review boards, and all subjects gave written, informed consent.

2.1.2 HIV-1 retrovirus

VSV-g pseudotyped virions HEK293T cells were transfected with pHDM-G vsv-g plasmid (generously provided by Dr. Jeng-Shin Lee, Harvard Gene Therapy Initiative) and pNL4-3 (from Dr. Malcolm Martin, (Cat #114) through the AIDS Research and Reference Reagent Program, Division of AIDS, NIAID, NIH) or pBR43IeG-nef$^+$ (from Dr. Frank Kirchhoff, (Cat #11349) through the AIDS Research and Reference Reagent Program, Division of AIDS, NIAID, NIH) according to manufacturers' instructions. Viral supernatant was harvested after 48 hr and stored in aliquots at -80°C.

JR-CSF Activated CD4$^+$ T cells were infected with JR-CSF (1-2 ng of p24 per 10^6 CD4$^+$ T cells) and incubated for 3-6 days. Viral supernatants were stored in aliquots at -80°C.

2.1.3 Primary CD4$^+$ T cell targets

CD8 cells were separated from PBMCs by positive selection (EasySep, StemCell Technologies) and non-CD8 cells were activated with anti-CD3:8 (gift from Johnson T. Wong, Center for

Prevention Research and the UCLA AIDS Institute, David Geffen School of Medicine at UCLA), anti-CD28 (R&D Systems), and IL-2 for 5-7 days. Where indicated, $CD4^+$ T cells were pulsed with (SL9 (SLYNTVATL, or variants) for which 1 nM peptide is equivalent to 1 ng/mL; KK10 (KRWIILGLNK) for which 1 nM peptide is equivalent to 1.25 ng/mL) for 1 hr at 37°C and washed. Alternatively, $CD4^+$ T cell targets were spinfected in R10/50 with polybrene (8 μg/mL) and HIV-1 (MOI of 0.001 to 0.1) at 37°C, 2400 RPM (1220 g) for 2 hr and washed. For imaging studies, infected targets were used 3 days post-infection when ~30% of the targets were infected ($p24^+$ by flow cytometry) as either sorted, GFP^+ and GFP^- populations, or unsorted. For viral inhibition assays, infected cells were used immediately after spinfection.

2.1.4 CTL clones

The A02-SL9 (gag p17) specific clone, 161jxA14, and the B27-KK10 (gag p24) specific clone, E501, are previously described (Chen et al., 2009; Collins et al., 1998). They were maintained in culture with periodic restimulation (Chen et al., 2009; Collins et al., 1998), and used in assays 12-20 days post-restimulation. For imaging, CTLs were stained with 5 μg/mL Alexa 647-CTXB (Invitrogen) for 30 min at 37°C, 5% CO_2, washed twice and resuspended in R10/50. For calcium imaging, CTLs were simultaneously labeled with CTXB and Fura-2 AM (Invitrogen) at 20 μg/mL for 20 min at 37°C, 5% CO_2 and imaged according to the manufacturer's instructions.

2.1.5 Primary polyclonal HIV-specific $CD8^+$ T cells

Strength and breadth of the Gag-specific CTL response is correlated with viral suppression *in vivo* (Barouch et al., 2010; Kiepiela et al., 2007). Thus, we chose to examine primary CTL from individual 285873 (HLA type A0201/A0301, B5101/B5101, Cw1402/Cw1502) with low viral loads (<75 virions/mL) in the absence of medication. This individual, classified as an elite

controller, exhibited a notably strong CTL response compared to other HIV$^+$ individuals in traditional ELISPOT assays. CD8$^+$ T lymphocyte epitope mapping indicated a particularly strong A2-SL9 specific CTL response (3600 SFC/10^6 PBMCs). The CTL response was also notably broad, recognizing overlapping 18-mer peptides from Gag (26 out of 48), Nef (9 out of 13), Tat (5 out of 6), Pol (8 out of 24), Vpr (0 out of 4), Env (1 out of 14), Vif (0 out of 3). The response to optimal peptides was measured and CTL recognition was broad [A2-SL9 (gag), A3-KK9 (gag), A3-RK9 (gag), A3-RY10 (gag), Cw14-LL8 (p17), A2-VV9 (p24), A3-TK10 (gp120), A3-RR11 (gp41), A2-SAV10 (env), A3-QK10 (nef), B51-LI9 (int), B51-EI9, (vpr), B51-LI9 (gp160)]. CD8$^+$ T cells were enriched from thawed PBMCs by negative selection (EasySep, StemCell Technologies) and primed with HLA-matched CD4$^+$ T cell targets pulsed with pools of overlapping 18-mer peptides representing HIV-1 proteins (Gag, Pol, Nef, Env). Cultures received IL-2 (50 U/mL) on days 2, 5 and 12.

2.1.6 Antigen presenting beads as target cell mimetics

Streptavidin beads (10 μm in diameter, CP01N, Bangs Labs) and biotinylated monomeric peptide-MHCI complexes (KRWIILGLNK, HLA-B*2705: Dale Long, NIH Tetramer Core Facility, Emory University) were rotated for 2 hr at 4°C, washed and used immediately. The density of peptide-MHCI on the surface of beads was quantitated by staining with PE-HLA-ABC (BD Biosciences) and comparing to Quantum Simply Cellular anti-Mouse IgG beads (Bangs Labs, 815) according to the manufacturer's instructions and was 20 pMHC/μm^2.

2.1.7 Three-dimensional fibrillar collagen gel model of peripheral tissue

Collagen mix was prepared on ice as follows: 180 μl of 0.1 M NaOH (sterile filtered) was aliquotted into a 5 ml tube. Next, 1440 μl of PureCol Collagen (Advanced Biomatrix, 5005, ~3.2 mg/mL) was added and vigorously pipetted, followed by 180 μl of 10x RPMI, 180 μl of fetal

calf serum, and 60 µl sytox green (Invitrogen, 5 mM source stock diluted to 40 µM in R10 just prior to use). The collagen mix was thoroughly pipetted, then rested at 4°C for >30 minutes prior to addition of cells. 340 µl of cold collagen mix was added to 30 µl of a target cell suspension, gently mixed by pipet, then transferred to 30 µl of a CTL suspension. The 400 µl samples (30 effector: 30 target: 340 collagen mix, v:v:v) were prepared and loaded into the center 4 wells of a warm 8 chambered labtek slide (Nunc, 155411) within 10 minutes and centrifuged down (~300 g, 3 min) to a single plane for imaging. The samples were seated in the environmental chamber on the motorized stage of the microscope and imaging was immediately initiated.

2.2 Assays of CTL Effector Functions

2.2.1 ^{51}Chromium cytolysis assays

$CD4^+$ T-cell targets were ^{51}Cr labeled (250 µCi/mL) and peptide-pulsed for 1 hr at 37°C. Liquid and 3D collagen assays were performed in triplicate in round-bottom 96 well plates at an E:T ratio of 1:1 ($1x10^4$ cells each) in a total volume of 200 µl. Co-cultures and controls (MaxR, targets lysed with 3% Triton-X 100; SR, targets alone) were packed by centrifugation (3 min, 300g) and incubated at 37°C, 5% CO_2 for 4-6 hours prior to supernatant collection. ^{51}Cr was measured on a Packard Topcount in counts per minute (CPM). ^{51}Cr release data was analyzed by nonlinear regression and EC_{50}s were calculated in Prism (Graphpad Software), % killed = (CPM-mean SR)/(mean MaxR CPM- mean SR CPM)*100.

2.2.2 Timelapse fluorescence microscopy assay for CTL killing

8-well chambered coverglasses (Labtek, Nalge Nunc) were coated with 100 µg/ml fibronectin in PBS for 18 hr at 4°C, and washed just prior to use. Neutral solutions of type I bovine collagen (PurCol 5005, Advanced Biomatrix) containing sytox green (Invitrogen, 5 µM in the final gel),

RPMI, 10% FCS were prepared following the manufacturer's instructions on ice. Cell suspensions (40,000 effectors, 40,000 targets within 400 μL neutral collagen) were deposited in pre-warmed (37°C) coverglasses, centrifuged at 300x*g* for 3 min, and imaging was immediately initiated at 37°C, 5% CO_2. Collagen samples were loaded in an environmental chamber maintaining 37°C, 5% CO_2 on a Zeiss Axiovert 200 epifluorescence microscope. Three images (sytox, CTXB, brightfield) were collected every 1 min at 20X or 40X for 4 adjacent stage positions in 4 parallel samples per imaging run (total field of view 1340 x 1800 μm per sample).

2.2.3 Timelapse fluorescence microscopy assay for intracellular, antigen-dependent TCR signaling

For calcium imaging, CTLs were simultaneously labeled with CTXB and Fura-2 AM (Invitrogen) at 20 μg/mL for 20 min at 37°C, 5% CO_2 and imaged according to the manufacturer's instructions.

2.2.4 Effector cytokine/chemokine secretion assay

100,000 CTL effectors and 100,000 target cells were loaded into collagen with a final total volume of 40 μL in a flat 96 well plate. Cells were centrifuged at 300g for 3 minutes. After 2, 4, or 6 hours of incubation at 37°C, 5% CO_2, 200 μL of R10 was floated on top of the collagen and incubated at 37°C, 5% CO_2 for 15 minutes. 200 μL liquid supernatant was harvested and was analyzed for cytokines and chemokines using human flex sets for MIP-1α, MIP-1β, RANTES, IFN-γ, and IL-2 (BD Biosciences) according to the manufacturers instructions.

2.3 VIDEOMICROSCOPY INSTRUMENTATION

2.3.1 Microscope and environmental controls

Imaging was performed on a Zeiss Axiovert 200 epifluorescence microscope equipped with a high-speed motorized stage (permitting parallel acquisition of 4 adjacent fields in 4 sample wells

in <50 seconds, Ludl, MAC5000), an environmental chamber (Zeiss Heating Insert P, CTI-Controller 3700, and Tempcontrol 37-2 digital) for maintenance of physiological conditions (37°C, 5% CO_2), and a cooled CCD digital camera with megapixel resolution (CoolSnap HQ, Roper Scientific). Exposure of cells to excitation wavelengths was carefully tuned through short exposure time (1 ms for sytox, ~400 ms for CtxB) and reduction of the excitation aperture resulting in signal acquisition at the bottom limit of detection for the express purpose of mitigating the phototoxic effects of more standard exposure schemes used in traditional static or short-term timelapse imaging.

2.3.2 Image quality: Objectives, magnification, camera and pixel binning

Quantitative studies were performed using a 20x/0.8 Plan-APOCHROMAT objective (Zeiss) to facilitate imaging compatible with fine (micron) and gross (centimeter) stage movements and data was saved with 3x3 binning of pixels. Representative examples included in the supplemental videos were generated using a 40x/1.3 Oil DIC Plan-NEOFLUAR objective and 1x1 pixel binning.

2.3.3 Computer-assisted multi-parameter data acquisition

Acquisition of up to 70,000 images per experiment [3 wavelengths (sytox fluorescence, CtxB fluorescence, brightfield) x 16 stage positions x 120-1440 timepoints] was computer-driven (Metamorph software, Universal Imaging). Images were acquired at 1 min intervals for 2-24 hours.

CHAPTER 3. DEVELOPMENT OF A VIDEO-MICROSCOPY ASSAY FOR DIRECT OBSERVATION OF MOTILE CTL KILLING

3.1 *IN SITU* FLUORESCENCE REPORTERS FOR CONTINUOUS, NON-TOXIC IMAGING OF CTL-TARGET ENGAGEMENT DYNAMICS AND CELL-MEDIATED DEATH

To directly observe the long-term dynamics and function of CTLs and to address the impact of cellular motility on CTL effector functions, we developed a dual fluorescence videomicroscopy strategy. This approach was implemented for cells within 3D type I collagen gels known to support lymphocyte migration (Gunzer et al., 2004; Weigelin and Friedl, 2010; Wolf et al., 2003). HIV-specific CTLs (clones and primary polyclonal cells) were obtained from persons who spontaneously control HIV without the need for medication. Primary HLA-matched $CD4^+$ T-cells were chosen as targets based on their physiological relevance as the predominant, HIV-infected population *in vivo* (Haase, 2005), and were either pulsed with cognate epitopes or infected with HIV for use as targets *in vitro*. To distinguish CTLs from $CD4^+$ T-cells, $CD8^+$ cells were labeled with a fluorophore-conjugated, nontoxic B subunit of Cholera toxin (CTXB), shown for the representative HIV-specific clone 161jxA14, referred to as A14 **(Figure 3.1a)**. CTXB labeled primarily the extracellular surface and endocytic vesicles, without affecting CTL function in a standard chromium release assay **(Figure 3.1b)**. The collagen matrix was infused with a membrane-impermeable sytox dye, which selectively fluoresces upon binding to DNA, allowing in situ observation of dead cells as they acquired green fluorescence upon loss of membrane integrity **(Figure 3.1c)**. The CTXB and sytox tracers were chosen to avoid fluorophore-mediated free radical generation in the cytosol of live CTLs or live target cells during imaging. The fluorescence microscope was environmentally controlled (5% CO_2, 37 °C, >90% humidity) and maintained cell viability for at least 24 hrs during imaging **(Figure 3.1d,**

and data not shown). Notably, CTXB is commercially available in a variety of colors and we have found that this strategy of CTL labeling can be multiplexed to differentiate separate CTL populations encountering unlabeled target cells within a single well **(Figure 3.2)**.

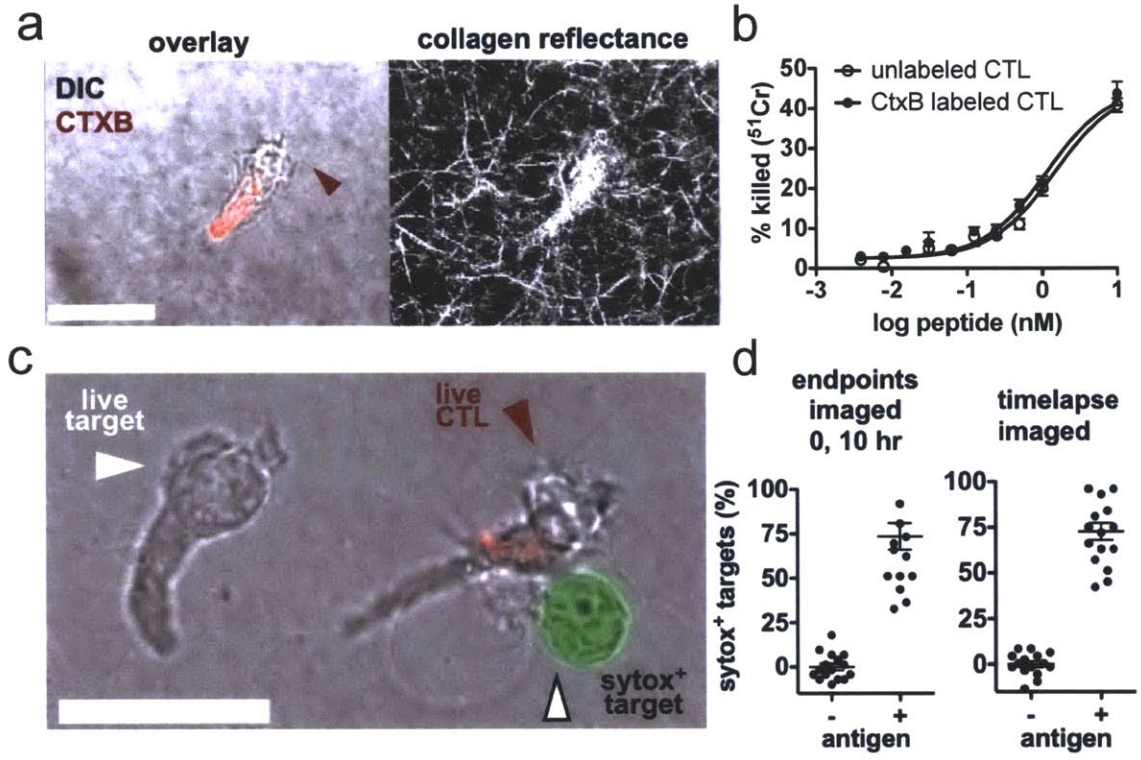

Figure 3.1. *In situ* reporters enabling faithful reporting of cell-mediated death and continuous videomicroscopy of CTLs and primary CD4$^+$ target cells in ECM.
(**a**) Confocal images of a CTL labeled with CTXB migrating through 3D fibrillar type I collagen gel (left: brightfield/CTXB fluorescence overlay, right: reflectance image of collagen fibers). Scale bar 20 μm. (**b-d**) A14 CTLs were co-cultured in ECM with HLA-matched CD4$^+$ T-cell targets pulsed with or without cognate peptide, as indicated. (**b**) CTXB labeling does not impair A14 CTL function in a traditional ^{51}Cr release assay. Shown is one representative of 2 independent experiments. (**c**) Image illustrating exclusion of sytox dye from live cells and in situ sensing of target permeabilization (2 nM SL9). Scale bar 20 μm. (**d**) A14 CTLs were co-cultured in ECM with targets (0 or 200 nM SL9) and samples were either imaged once at time 0 and once after 10 hr (left) or timelapse imaged at 1 min intervals for 10 hr (right). Target cell permeabilization was assessed by software-generated CTXB$^-$ sytox$^+$ cell counts. Shown is one representative of 4 independent experiments.

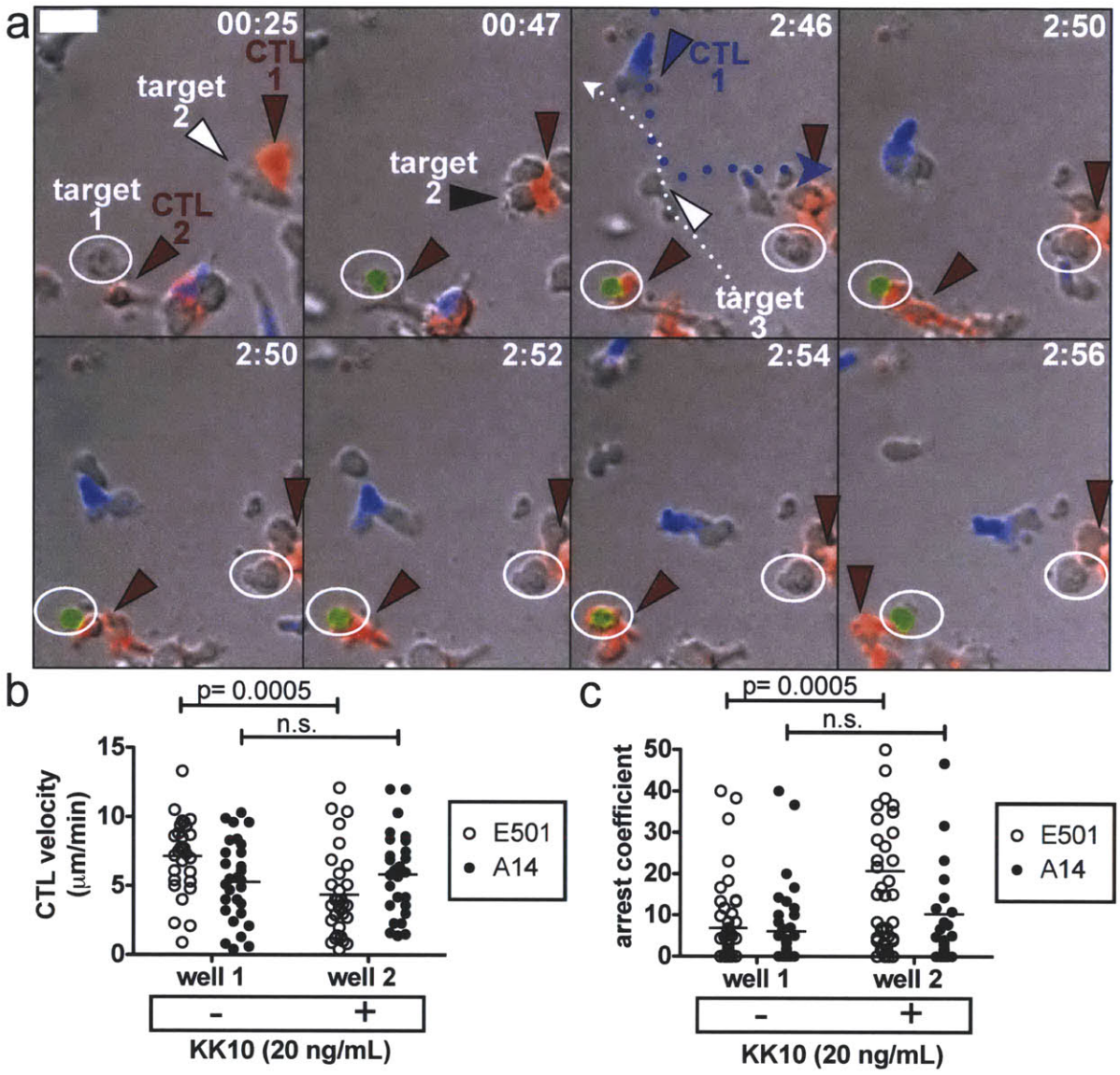

Figure 3.2. CTXB-fluorophore conjugates in different colors can be multiplexed to differentiate between three or more populations of cells.

E501 and A14 CTLs were labeled with Alexa-555 or Alexa-647 CTXB, respectively, and were co-cultured in ECM with unlabeled HLA-matched BCL target cells pulsed with KK10 peptide (cognate antigen for E501, but not A14 TCR) as indicated. (**a**) E501 CTLs (in red pseudocolor) are engaged in target killing while A14 CTLs (in blue pseudocolor) fail to engage BCL bearing irrelevant antigen. Three cell populations are indicated as follows: E501, red arrows and text; A14, blue arrow, text and dotted line for path of migration; BCL pulsed with KK10 (20 ng/mL), white text, white dotted line for path of migration, white arrows while live, black arrow while blebbing, and a white circles for killed targets. Permeabilized target is visualized in green with sytox. Scale bar 20 μm. Elapsed time indicated in hr:min. (**b, c**) E501 and A14 CTL migration was assessed for a 1-hour period beginning 2 hours after initiation of coculture and (**b**) CTL velocity and (**c**) arrest coefficients are shown.

3.2 Cell migration and transient CTL-target encounter within the 3D ECM tissue model

We next assessed the migration dynamics of HIV-specific CTLs and targets within this ECM tissue model in the absence of antigen. The Gag-specific CTL clone A14, and primary $CD4^+$ T-cell targets polarized and migrated within the matrix with a persistent random walk and mean velocities of 5-10 μm/min (**Figure 3.3a, Videos 1 and 2**), as expected (Friedl and Brocker, 2004; Gunzer et al., 2004; Weigelin and Friedl, 2010). At cell densities of 200 cells/μL gel and E:T ratio 1:2, CTLs encountered targets with a mean hit rate of ~2 targets per hour (**Figure 3.3b**), but without antigen these contacts were transient (median time 7.2 min, **Figure 3.3c**) and did not involve changes in CTL or target velocity.

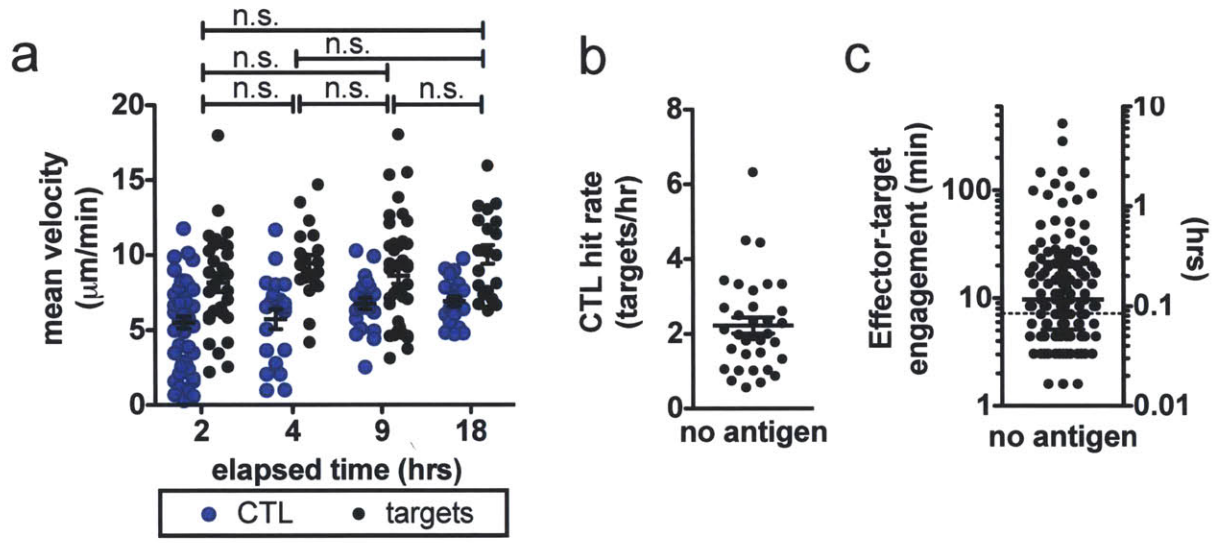

Figure 3.3. Cellular dynamics within extracellular matrix.
A14 CTLs were cocultured in ECM with HLA-matched $CD4^+$ targets in the absence of cognate peptide and imaged continuously for 20 hrs. (a) The mean velocity of individual CTLs and targets for the indicated one-hour periods are shown. Bars indicate mean ± SEM. (b) Number of targets encountered by individual CTL per hour. Bars indicate mean ± SEM. (c) Duration of individual CTL-target engagements. Dotted line indicates the median.

3.3 CTL LYTIC FUNCTION WITHIN THE 3D ECM TISSUE MODEL

We next confirmed the anti-viral activity of two HIV Gag-specific CTL clones within this ECM tissue model. Since the ultimate goal is to define characteristics of effective CTL function, we chose to examine two clones derived from elite controllers of HIV who spontaneously control virus without medication (Chen et al., 2009; Collins et al., 1998). Clone 161jxA14 (hereafter, A14) is restricted by HLA-A*0201, the most common Caucasian class I allele, and clone E501 is restricted by HLA-B*2705, an allele associated with protection from HIV disease progression (Kaslow et al., 1996). Both clones readily killed peptide-pulsed, HLA-matched $CD4^+$ T-cell targets in 3D collagen matrices and in liquid culture, but differed substantially in peptide sensitivity, with half-maximal killing by the A14 clone achieved at >20-fold lower doses of antigen (**Fig. 3.4a, b**). Thus, CTLs readily demonstrated functional activity in this ECM model where both CTLs and target cells exhibit rapid migration dynamics.

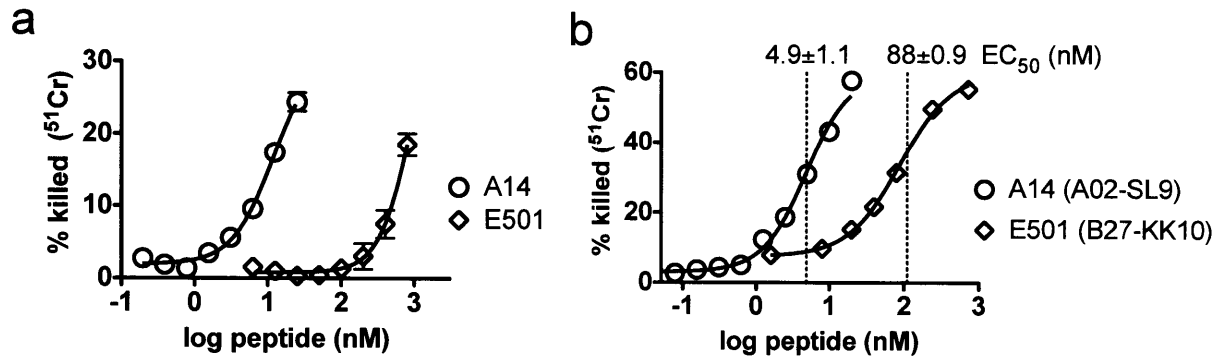

Figure 3.4. Antigen-dependent CTL function is preserved within the 3D ECM tissue model
Gag-specific CTL clones A14 and E501 were co-cultured with ^{51}Cr–labeled, HLA-matched $CD4^+$ T cell targets pulsed with indicated doses of cognate HIV Gag peptide (SL9 or KK10, respectively; E:T ratio 1:1) and ^{51}Cr release was measured after 6 hrs (**a**) in collagen and (**b**) in liquid suspension.

3.4 A HIGH-SPEED MOTORIZED STAGE SUPPORTS AUTOMATED ACQUISITION OF INTERNALLY CONTROLLED TIME-LAPSE MICROSCOPY DATA SETS

Traditional epifluorescence microscopy is conducted with an emphasis on generating high-quality images at magnifications (40x to 100x) sufficient to resolve protein distributions on the subcellular level. Images are frequently collected manually for multiple samples at a single timepoint. The goal of this work was quite distinct and thus required a substantially different approach. In order to characterize the antigen-dependent dynamics of migrating CTLs encountering motile target cells, it was imperative that we generate internally controlled data sets by acquiring data on experimental and control samples prepared in parallel. We chose to use a 20x air objective, knowingly sacrificing nanometer-scale resolution traditionally acquired with higher magnification oil objectives, with the intent of supporting gross (centimeter scale) stage movements. We employed multidimensional data acquisition software and a high-speed motorized stage to facilitate rapid serial imaging of up to four samples, thus ensuring that all experiments were internally controlled (**Figure 3.5**). Data was collected for each well at 4 adjacent stage positions to increase the number of encounters observed and to increase the field of view.

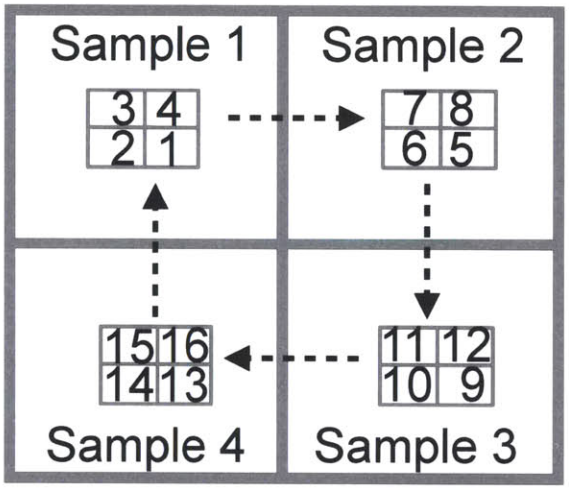

Figure 3.5. Rapid serial imaging of up to four samples produces internally controlled data sets.

A high-speed motorized stage facilitated acquisition of 4 adjacent fields of view of 4 parallel samples. Fluorescence (sytox, CTXB) and brightfield images were collected every 1 min at 20X or 40X magnification for 2-24 hrs. Total field of view 1340 x 1800 μm per sample.

3.5 CONCLUSIONS

We have developed an epifluorescence videomicroscopy approach for monitoring cell-mediated death and differentiating between distinctly labeled populations of cells migrating in 3D ECM coculture. Continuous videomicroscopy without evidence of phototoxicity was achieved with our strategically chosen *in situ* reporters for periods ~25x longer than those achieved with intravital imaging. Furthermore, to our knowledge, this approach is unique in its ability to support continuous observation of primary $CD4^+$ T cells which are more sensitive to phototoxicity (data not shown) than the EBV-transformed B cell lines or tumor cell lines frequently used as targets in bulk assays or other videomicroscopy assays of cell-mediated death (Keefe et al., 2005; Purbhoo et al., 2004; Wiedemann et al., 2006; Yang et al., 2003).

CHAPTER 4. HIV-SPECIFIC CTL FUNCTION WITHIN A 3D EXTRACELLULAR MATRIX MODEL OF PERIPHERAL TISSUE

4.1 MIGRATING HIGH-AVIDITY CTLS SHOW HIGH EFFICIENCY IN TARGET RECOGNITION AND KILLING AT THE SINGLE-CELL LEVEL

To directly observe antigen-dependent CTL dynamics and killing, A14 CTLs were co-cultured in ECM with primary HLA-matched $CD4^+$ targets pulsed with cognate SL9 peptide (SLYNTVATL, p17 amino acids 77 to 85) or SL9 variants. The frequency of SL9-pulsed targets killed by A14 CTLs as detected by sytox fluorescence after 10 hr was antigen dose-dependent (**Figure 4.1a**). While antigen dose- and functional avidity-dependent target death at the population level is expected, the impact of these antigen recognition parameters on the response of CTLs at the single-cell level is unknown. We identified a panel of SL9 peptide variants known to bind equivalently to HLA-A2 (Iversen et al., 2006), for which A14 CTLs exhibited a broad range of functional avidity as determined by a bulk chromium lysis assay in collagen; in addition, we tested a second Gag-specific CTL clone E501, also obtained from an HIV elite controller (**Figure 4.1b**). We then quantified the efficiency with which individual CTLs recognized and killed the first target cell contacted in the collagen matrix, exploiting the SL9 variants to modulate functional avidity in the absence of inter-clonal differences. Strikingly, A14 CTLs exhibited first-contact kill efficiencies of >90% in response to targets pulsed with low concentrations (1-10 nM) of the SL9 peptides recognized with high avidity (single mutant or wild-type). However, these same CTLs were remarkably inefficient during engagement of targets bearing lower avidity peptides, requiring ~10- and ~1000-fold higher doses of double mutant or triple mutant peptides, respectively, to achieve comparable engagement efficiencies (**Figure 4.1c**). E501 CTLs, restricted by HLA-B*2705, had ~65-fold lower avidity for their cognate peptide than A14 CTLs

and required nearly 100-fold higher antigen doses to achieve >50% first-contact-kill efficiency (**Figure 4.1b, c**). Thus, migrating CTLs require high avidity TCRs to efficiently recognize, engage, and kill migrating target cells on first contact, particularly under conditions of limiting antigen doses most relevant to physiological conditions.

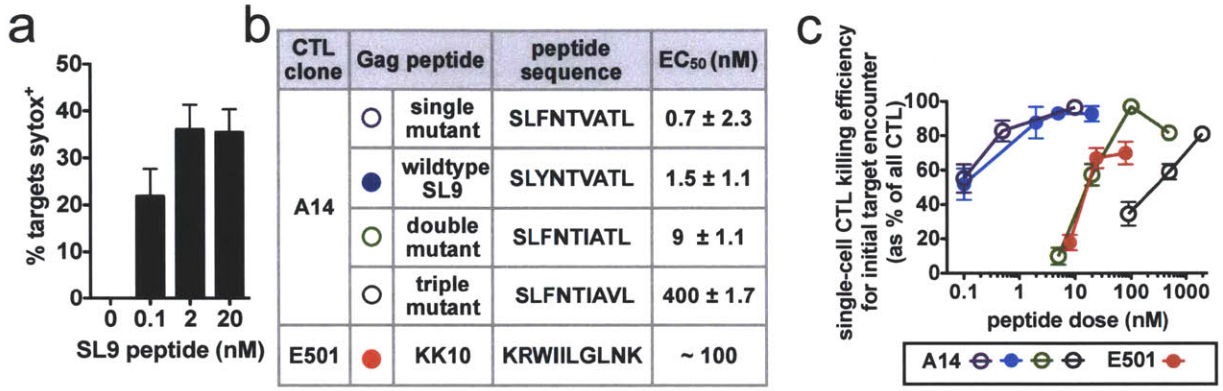

Figure 4.1. Videomicroscopy reveals the single-cell efficiency of CTL killing, highlighting a new role for TCR avidity in capturing migrating targets.
CTL clones were co-cultured in ECM with HLA-matched $CD4^+$ targets pulsed with the indicated concentrations of cognate antigen (1:2 E:T ratio). (**a**) $Sytox^+$ targets were enumerated after 10 hr of co-culture with A14 CTLs and expressed as a % of live targets in view at time 0. (**b**) ^{51}Cr release from targets was measured for CTLs co-cultured with peptide pulsed targets after 6 hr within ECM. EC50s indicate functional avidities. (**c**) The percentage of individual CTLs that killed the first target cell encountered as determined by videomicroscopy.

We next characterized the dynamics of CTL-target interactions during killing. Within a single sample, successful CTL-target engagements for clone A14 encountering HLA-matched targets fell into two characteristic categories (**Figure 4.2a, b**): During "direct hit kills", CTL engagement with a motile target triggered immediate motility arrest of both the effector and target cell, followed by rapid target cell death (**Figure 4.2a**, **Video 3**, first segment). In rarer instances, CTL engagement of a target was marked by continued target cell migration away from the arrested CTL, often pulling a long tail of target cytoplasm as it migrated, before the tethered

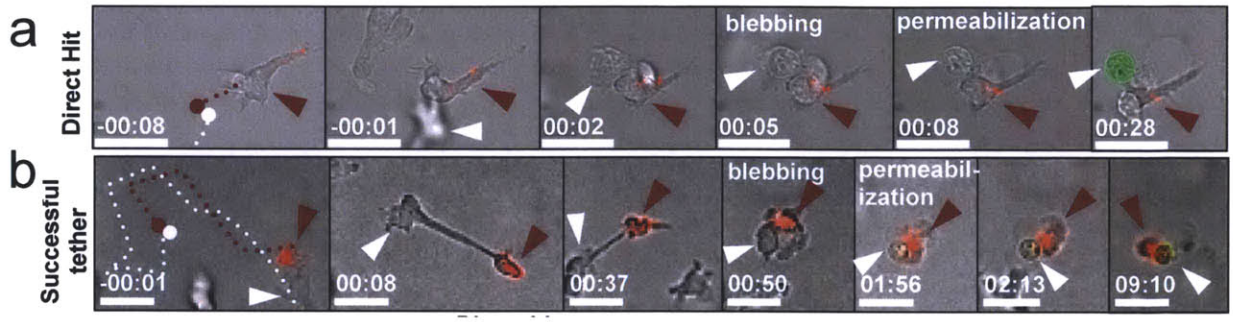

Figure 4.2. Characteristic examples of CTL-target engagement dynamics within ECM. A14 CTLs were co-cultured in ECM with HLA-matched $CD4^+$ targets pulsed with cognate antigen (2 nM SL9 peptide, 1:2 E:T ratio). Serial images from representative CTL killing events: (**a**) direct hit kill, (**b**) successful tether. Scale bars 20 μm; elapsed time from initial engagement (hr:min). Cells and paths of migration are marked with dotted lines and/or arrows in red (for CTL) or white (for targets).

target eventually stopped forward motion, blebbed, and snapped back to the CTL as it was killed ("successful tethers," **Figure 4.2b**, **Video 3**, second segment). Successful tethers involved prolonged struggles and delayed signs of target death, with a mean duration of 1.3 hr, whereas direct hits typically progressed to target death in less than 20 min (**Figure 4.3a**). Imaging of A14 CTLs labeled with Fura-2 AM showed that calcium flux was rapid and coincident with CTL migration arrest for both direct hit kills and successful tethers. Direct hits were accompanied by stronger Ca^{++} signaling, characterized by Fura ratio changes of greater amplitude and duration, which persisted post-target death (**Figure 4.3b** and **Video 4**). Once targets were engaged, CTL killing in ECM followed kinetics similar to those measured in liquid cultures (Purbhoo et al., 2001; Stinchcombe et al., 2001), with blebbing observed ~30 min after target engagement and targets permeabilized after ~3 hr (**Figure 4.3c**). Similar CTL-target engagement dynamics and killing kinetics were observed for the E501 CTL clone (data not shown). Thus, the majority of successful kills were accompanied by immediate arrest of both the migrating CTL and target cell, followed by blebbing in the target cell indicating delivery of a lethal hit in less than 1 hr.

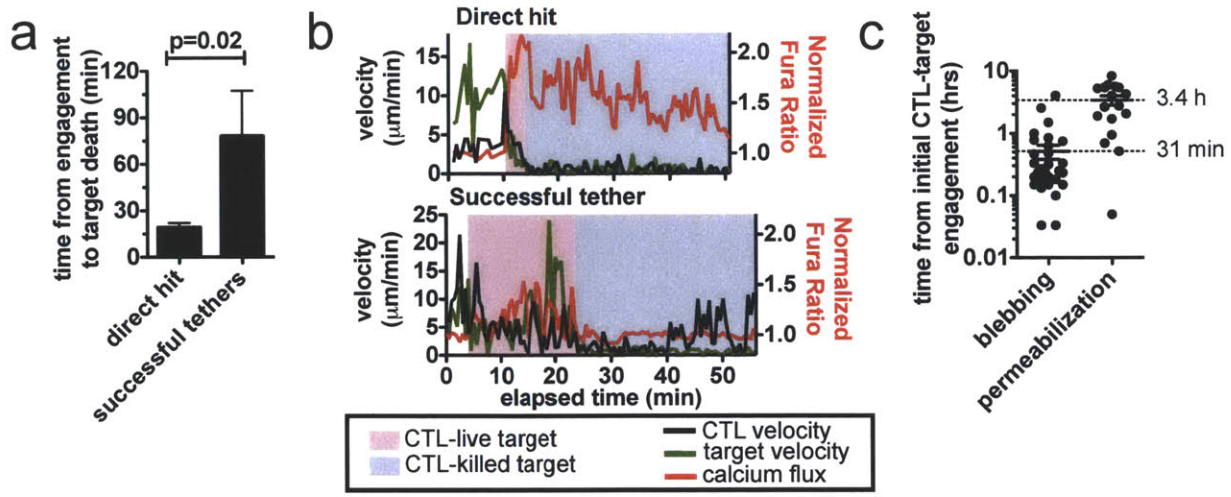

Figure 4.3. Migrating CD4⁺ T-cell targets are rapidly engaged and killed by CTLs.
A14 CTLs were co-cultured in ECM with HLA-matched CD4⁺ targets pulsed with the indicated concentrations of cognate antigen. (**a**) Duration of CTL-target engagement until target death depending on engagement type (20 nM SL9). (**b**) Ca^{2+} signaling was monitored in A14 CTLs loaded with FURA-2 AM and traces are shown (red) for characteristic CTL killing events (2 nM SL9). Velocity traces (CTL in black, target in green) and CTL engagement with live target (pink) and killed target (gray) engagement are denoted on the time axis. (**c**) Duration from initial engagements until blebbing, permeabilization for all killed targets (20 nM SL9). (**a, c**) One representative of 3 independent experiments. Bars indicate mean ± SEM.

4.2 Motile targets escape in ECM, reducing the killing efficiency of low-avidity CTLs

Prompted by the poor single-cell efficiency of target killing elicited by low-avidity TCR-peptide interactions (**Figure 4.1c**), we next asked whether target motility *per se* influences target recognition. Under conditions of both low and high first-contact target killing efficiency, we also observed a fraction of motile targets actively escaping CTLs (**Figure 4.4**). These failed engagements fell into two characteristic categories: During "failed tethers" CTLs arrested and tethered a target, but the CD4⁺ cell continued to migrate, pulling long tails of target cell cytoplasm before escaping (**Figure 4.5a**, **Video 5**, first segment). "Brushes" were defined as apparent contact between a motile antigen-bearing target and an A14 CTL, without CTL arrest or reorientation of the CTL toward the target (**Figure 4.5b**, **Video 5**, second segment).

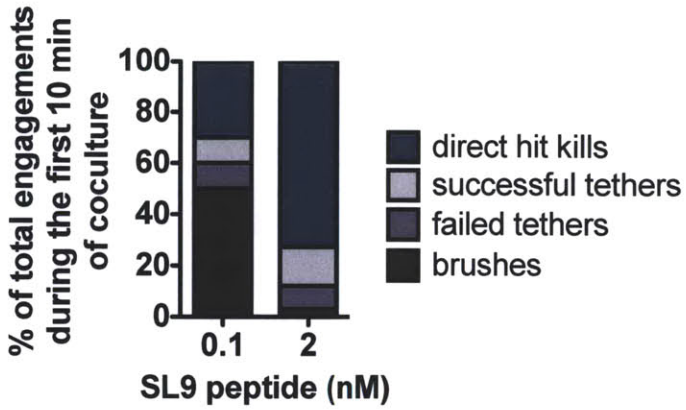

Figure 4.4. Targets escape CTLs under conditions of both low and high first-contact target killing efficiency.

CTL clone A14 was co-cultured with HLA-matched $CD4^+$ targets pulsed with cognate SL9 peptide (1:2 E:T ratio) in collagen gels. Analysis of the first 10 minutes of videomicroscopy revealed characteristic CTL-target engagements, direct hit kills, successful tethers, failed tethers, and brushes with greater frequencies of target escape occurring under conditions of low (0.1 nM SL9) first-contact efficiency relative to high (2 nM SL9) first-contact efficiency.

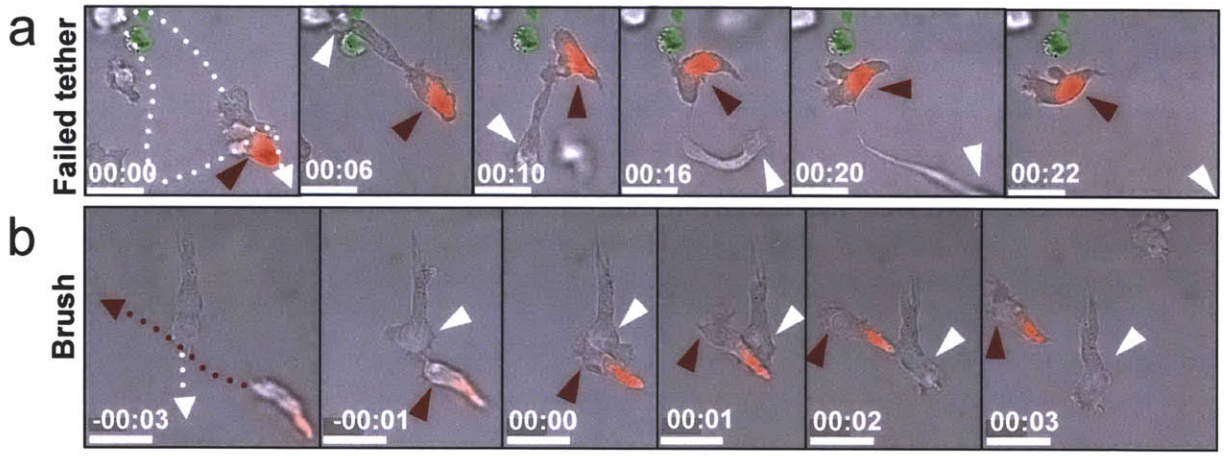

Figure 4.5. A fraction of CTL-target encounters in ECM conclude with motile target escape.

CTL clone A14 was co-cultured with HLA-matched $CD4^+$ targets pulsed with the indicated concentrations of SL9 peptide in collagen gels (1:2 E:T ratio). (**a, b**) Serial images from representative examples of characteristic target escape events (target cells pulsed with 2-10 nM SL9 peptide): (**a**) failed tether, (**b**) brush. Scale bars 20 μm; elapsed time shown in (hr:min). Cells and paths of migration are marked with dotted lines and/or arrows in red (for CTLs) or white (for targets).

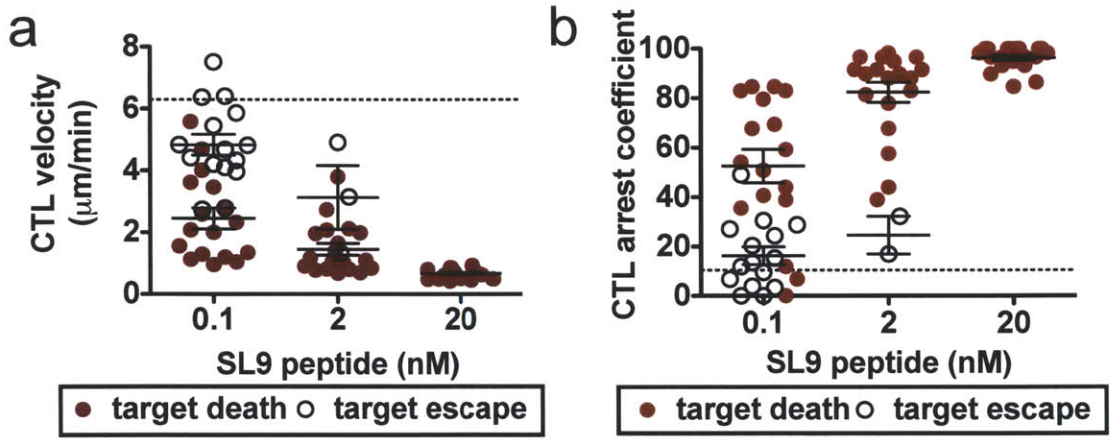

Figure 4.6. CTL migration arrest is tightly associated with target killing activity.
CTL clone A14 was co-cultured with HLA-matched $CD4^+$ targets pulsed with the indicated concentrations of SL9 peptide in collagen gels (1:2 E:T ratio). (**a**) The mean velocity of individual CTLs from hours 1-2 of imaging is indicated for CTLs observed to encounter and kill or fail to kill targets. (**b**) Arrest coefficients were calculated for the CTLs analyzed in (**a**). Arrest coefficient is defined as the percentage of time that a CTL exhibits an instantaneous velocity of <2 μm per one minute interval. Dotted lines on the y-axis mark the mean velocity/arrest coefficient of CTLs in the presence of targets in the absence of cognate antigen. Data are from one representative of 3 independent experiments. Bars indicate mean ± SEM.

Tracking of CTLs during hours 1-2 of imaging revealed that arrest of CTL migration is tightly associated with TCR signaling and target killing activity since antigen dose-dependent decreases in mean CTL velocity and increases in arrest coefficient were observed for CTL-target engagements resulting in target cell death (**Figure 4.6a, b**). Direct examination of TCR triggering kinetics and calcium flux in the context of these cellular dynamics revealed that failed tethers were frequently marked by weak calcium signals and brief CTL migration arrest, which terminated prior to target cell escape and a return of CTL motility; and signaling was largely

absent during brushes (**Figure 4.7a**, **Video 6**). Although calcium signaling was consistently present during engagements marked by lethal hit delivery, CTLs fluxed calcium during only ~70% of failed tethers and ~10% of brushes (**Figure 4.7b**). Death progressed with similar kinetics whether targets received a lethal hit following escape from multiple CTLs or from the first CTL encountered, suggesting that failed CTL contacts did not inflict cumulative, sub-lethal damage (**Figure 4.7c**).

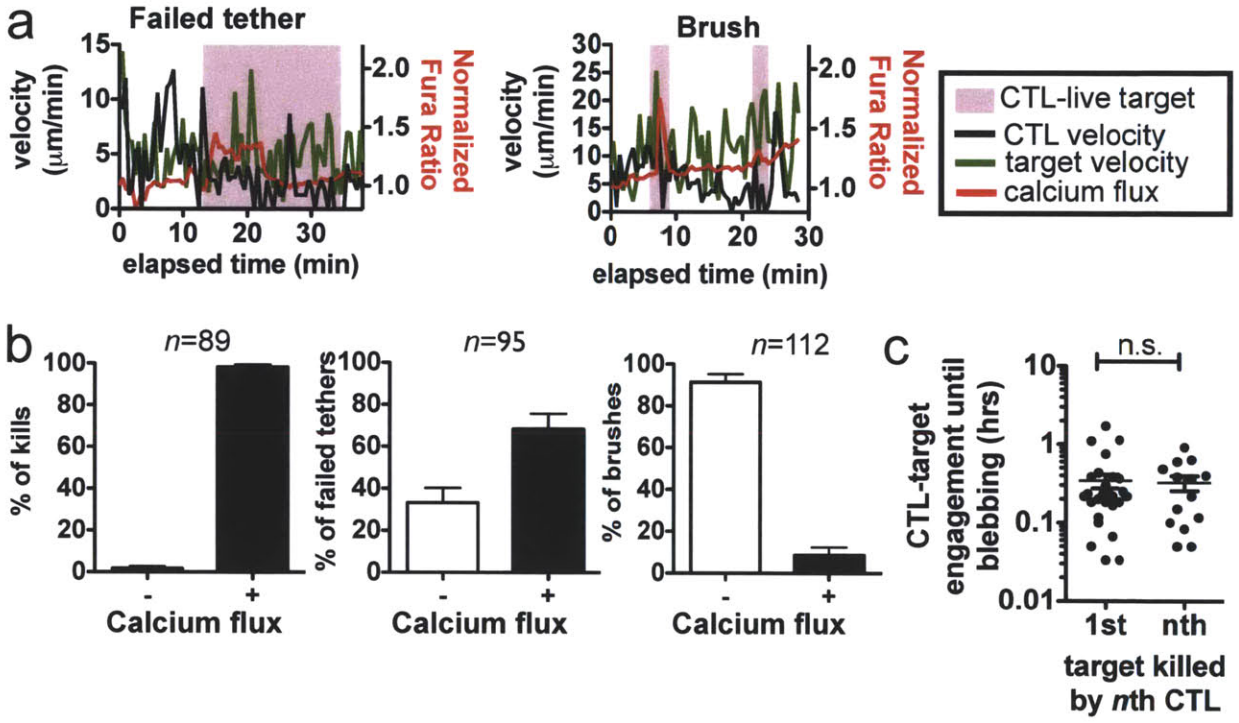

Figure 4.7. Failed CTL-target engagements are marked by weak or absent TCR signals and motile target escape.

CTL clone A14 and HLA-matched CD4$^+$ targets pulsed with the indicated concentrations of cognate peptide were co-cultured in collagen gels (1:2 E:T ratio). (**a, b**) Calcium signaling was monitored in A14 CTLs loaded with FURA-2 AM (2 nM SL9). (**a**) Calcium signaling (red) and velocity traces (CTL in black, target in green) are shown for characteristic target escape events, including failed tethers (left) and brushes (right). CTL-engagement with a live target is denoted in pink on the time axis. (**b**) The percentage of CTL-target kills (left), failed tethers (middle panel) and brushes (right) exhibiting calcium signaling. (**c**) Duration of CTL-target engagement from initial contact until target blebbing for targets killed by the first or *n*th CTL encountered (20 nM SL9).

To directly address whether target motility contributes to the poor efficiency of low-avidity CTLs, we immobilized targets on the glass substrate at the base of collagen gels with anti-CD4 antibodies (**Figure 4.8a**). Low-avidity E501 CTL clones lysed 2.6-fold more immobilized target cells than freely motile target cells as measured by bulk sytox$^+$ nuclei counts after 10 hr ($p<0.001$, **Figure 4.8b**). Motile CD4$^+$ cells that were eventually killed broke contact and escaped a mean of 2.9 ± 0.4 CTLs prior to target death, but immobilized targets were typically killed upon their first encounter with a CTL (mean = 1.5, **Figure 4.8c**, $p=0.0021$). Thus, target cell migration affects the efficacy of CTLs, with weak target engagement by low-avidity CTLs permitting escape of migrating targets prior to delivery of a lethal hit.

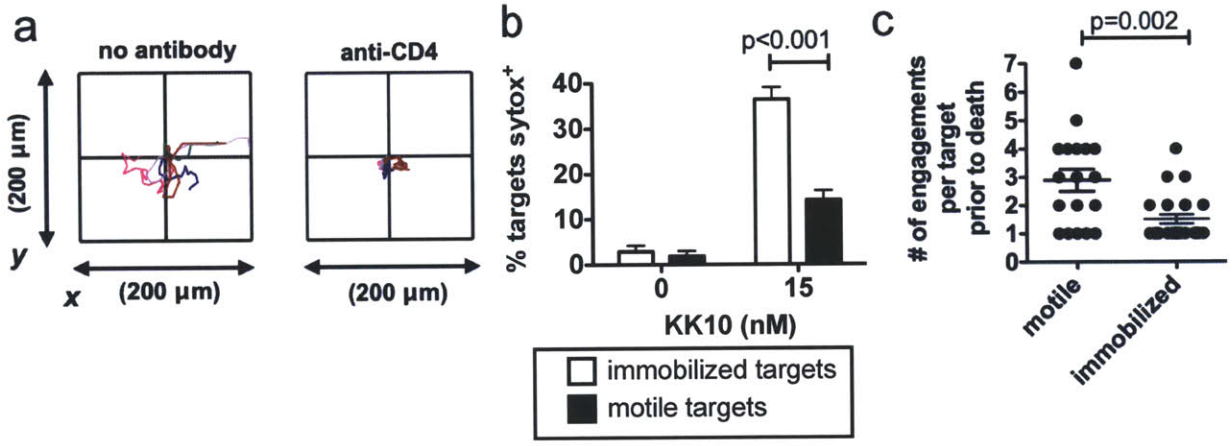

Figure 4.8. Target cell motility directly impacts CTL killing and promotes target escape. Lower avidity E501 CTLs and CD4$^+$ T cell targets pulsed with the indicated concentrations of cognate peptide (E:T ratio 1:2) were gently centrifuged through collagen precursor solutions onto a glass substrate coated with anti-CD4 capture antibodies to immobilize targets prior to collagen gelation and compared to controls lacking anti-CD4. (**a**) Wind-rose plots of individual target cell migration paths were tracked over a period of 20 minutes. (**b**) Target cell death after 10 hr of imaging was assessed by sytox fluorescence and (**c**) engagement histories were recorded for motile or immobilized targets that were killed during the observation period.

4.3 KILL-EXPERIENCED CTLS ARREST FOR HOURS AND FAIL TO KILL SUBSEQUENT TARGETS

Exploiting our ability to record both initial target contact and long-term cellular dynamics (**Figure 4.9**), we next characterized the kinetics of sequential CTL engagement with targets over a 10 hr period. Notably, A14 CTLs exhibited prolonged engagements with the first $CD4^+$ cell killed. These dynamics were antigen dose-dependent, with target engagement lasting ~5 hr on average at doses eliciting nearly 100% first-contact kill efficiencies (**Figure 4.10a, b**). Often, the CTLs migration did not resume random walk migration for hours even after contact with a killed target was broken, as indicated by arrest coefficients (% of time CTL velocity <2 μm/min) (**Figure 4.10b** and **Figure 4.9**, **Video 7**, first segment).

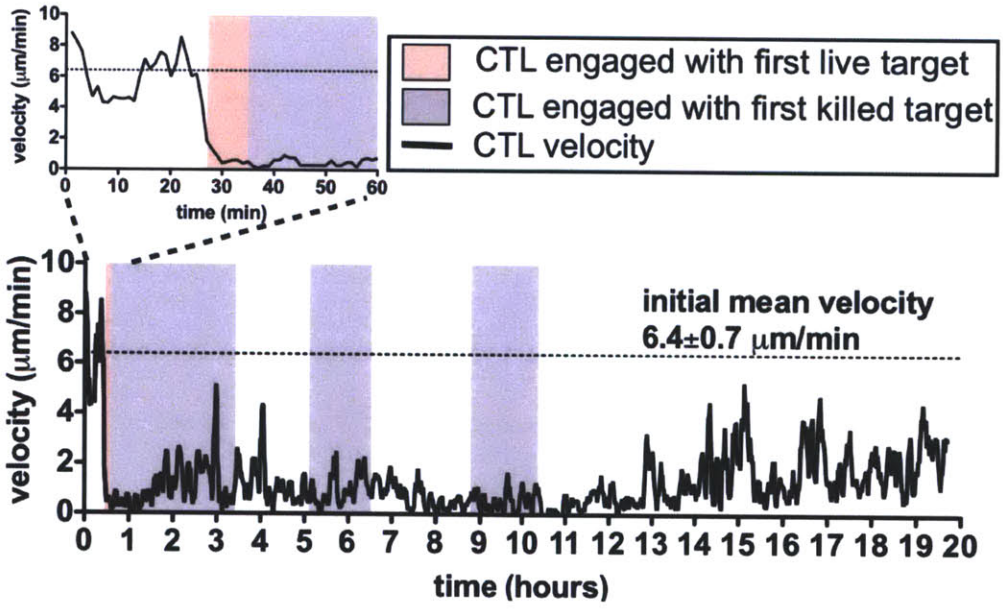

Figure 4.9. Continuous observation of an individual CTL for 20 hours reveals initial target contact and long-term cellular dynamics.
E501 CTLs were imaged engaging HLA-matched targets pulsed with KK10 peptide (100 ng/mL) in collagen matrices. Instantaneous velocities, calculated based on 1 min intervals, for an E501 CTL for the entire 20 hr time period and (inset) for the first hour. CTL-engagement with a live target is denoted in pink on the time axis, and CTL engagement with dead target is denoted in gray. The mean velocity for this CTL before encountering and killing its target is indicated with a dotted line at 6.4±0.7 μm/min.

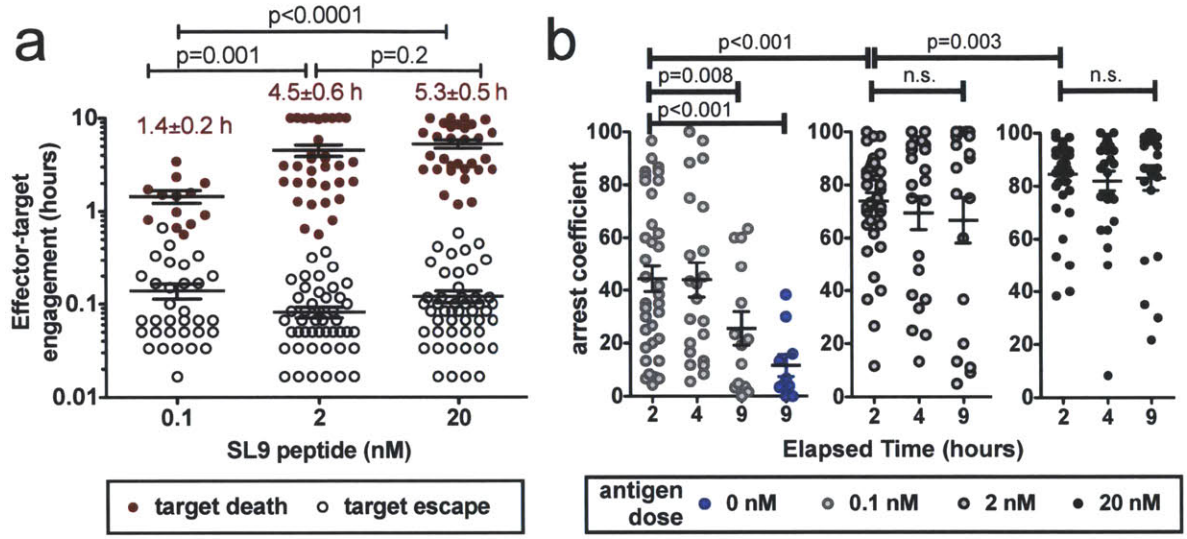

Figure 4.10. CTLs exhibit prolonged engagement and migration arrest upon killing.
A14 CTLs engaging $CD4^+$ T-cells pulsed with the indicated doses of SL9 peptide in collagen were imaged for 10 hr (E:T ratio 1:2). (**a**) Total engagement time for CTL-target encounters ending in target death or escape. (**b**) CTL arrest coefficients were calculated from 1 hr intervals after 2, 4, or 9 hr of co-culture as a function of antigen dose. Data shown from 1 representative of 3 independent experiments. Bars indicate mean ± SEM.

To determine whether TCR signaling alone is sufficient to elicit long-lived CTL arrest, we displayed recombinant B*27-KK10 peptide-MHC complexes on cell-sized beads. E501 CTLs exhibited arrest on beads bearing cognate antigen, but interacted only briefly with control beads (**Figure 4.11**). Thus, CTLs kill their first target within minutes, but TCR signaling induces a durable, CTL-intrinsic motility arrest and many hours of contact with dead targets.

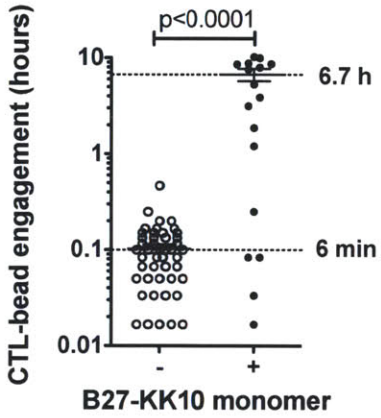

Figure 4.11. A CTL-intrinsic, TCR-dependent stop signal is sufficient to induce prolonged CTL arrest.
Cell-sized beads presenting recombinant B27-KK10 peptide-MHC complexes at a density of 20 pMHC/μm^2 and control beads lacking pMHC were prepared. The duration of E501 CTL engagements with beads in collagen was examined using videomicroscopy. Data from 1 representative of 4 independent experiments. Bars indicate mean ± SEM.

Strikingly, once A14 or E501 CTLs engaged and killed an initial target, ~90% of all contacts with subsequent targets over the following 8-10 hr were failures at all antigen doses, even at supra-physiological (μM) concentrations of peptide (**Figure 4.12** and data not shown). These post-first-kill failed engagements (brushes and failed tethers) were brief (~5-10 min) and account for nearly all of the target escapes recorded at the 2 and 20 nM peptide doses in **Figure 4.10a**. Although high-avidity A14 CTLs exhibited near-perfect efficiency in killing the first target encountered at 2 nM SL9, only ~25% of the $CD8^+$ cells killed any subsequently

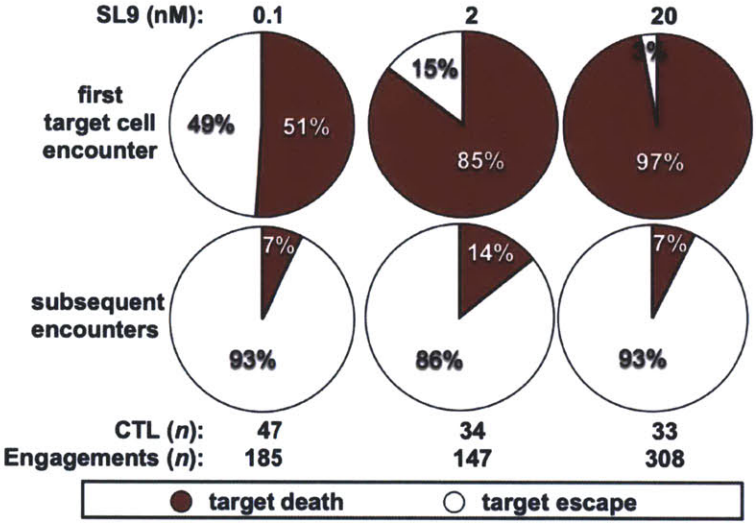

Figure 4.12. CTLs fail to engage or kill subsequent motile targets after efficiently killing their first-encountered target.

A14 CTLs were co-cultured with $CD4^+$ T-cells pulsed with the indicated doses of SL9 peptide in collagen and were imaged for 10 hr (E:T ratio 1:2). Outcomes for each CTL engaging its first target or subsequent targets are expressed as % of first CTL encounters or % of subsequent encounters. Data shown from 1 representative of 3 independent experiments.

encountered targets over 10 hrs (**Figure 4.13a**). This did not reflect a lack of contact with additional targets, as numerous live $CD4^+$ cells migrated over arrested CTLs, which were typically still engaged with their first dead target (**Figure 4.13b**). These failed contacts were observed as rapidly as 2 min following successful CTL engagement of the initial target (**Figure 4.14**, **Video 7**, second segment). Those CTLs that did successfully kill more than one target did so by capturing subsequent passing $CD4^+$ cells while still stopped and engaged with their first dead target (**Video 7**, third segment). This is illustrated quantitatively in **Figure 4.14** for the case of 20 nM SL9-pulsed targets; the mean time between lethal hits for CTLs killing multiple targets was 2.3 hr, while the mean total engagement with killed targets was ~5 hr (**Figure 4.10**). Similar results were obtained with the lower-avidity CTL clone E501 (data not shown). By contrast, a target-centric analysis of the outcome for all targets visible at the initiation of imaging indicate that while target deaths increase with antigen dose, the % of targets which never encounter a CTL also correlates with antigen dose as a consequence of prolonged CTL engagements with their initial killed target (**Figure 4.15**). Taken together, these data indicate that kill-experienced CTLs fail to kill new targets for many hours, under conditions of high and low initial efficiency, regardless of antigen density. Furthermore, since many targets to remain entirely unencountered following commitment to an initial target, these unencountered targets are free to escape.

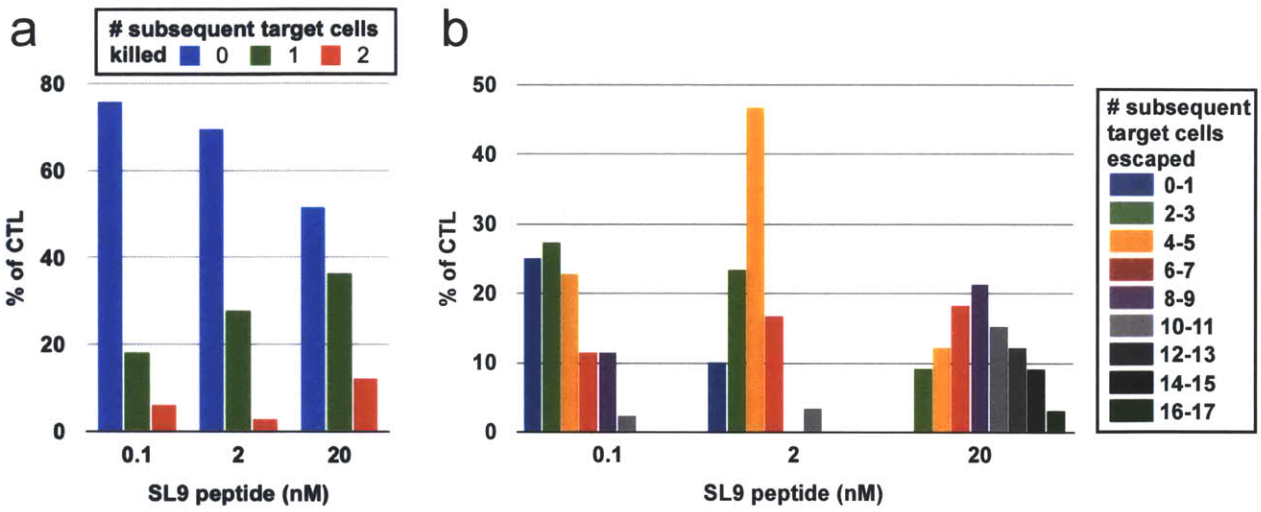

Figure 4.13. CTLs are refractory to killing subsequent targets, despite numerous subsequent target contacts.

A14 CTLs were co-cultured with $CD4^+$ T-cells pulsed with the indicated doses of SL9 peptide in collagen and were imaged for 10 hr (E:T ratio 1:2). (**a**) Enumeration of # of subsequent targets killed by individual CTLs over 10 hr following a first kill. (**b**) CTLs that killed an initial target were analyzed to enumerate the number of subsequent targets that contacted the CTL post-first-kill without receiving a lethal hit. Data shown from 1 representative of 5 independent experiments.

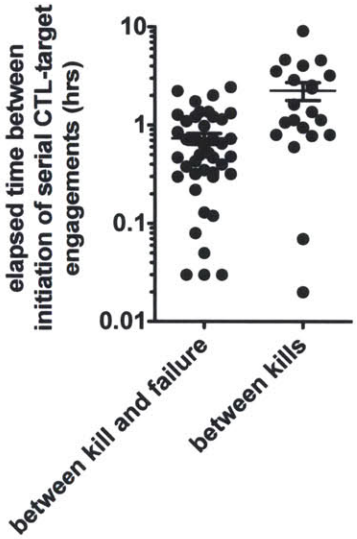

Figure 4.14. CTL contact with subsequent targets occurs while CTLs are still engaged with their initial target.

A14 CTLs were co-cultured with $CD4^+$ T-cells pulsed with the indicated doses of SL9 peptide in collagen and were imaged for 10 hr (E:T ratio 1:2). Elapsed time between initial target cell killing and subsequent target contacts for individual CTLs (20 nM SL9). Data shown from 1 representative of 3 independent experiments. Bars indicate mean ± SEM.

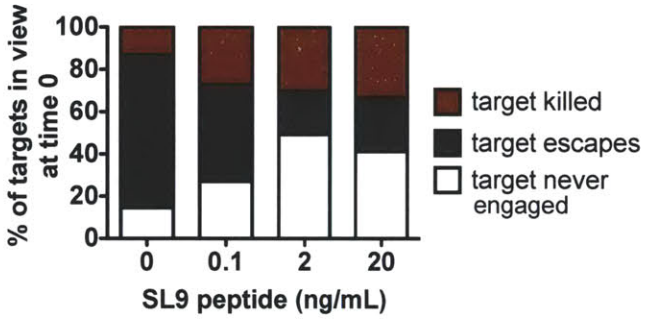

Figure 4.15. CTL killing and arrest correlates with an increased frequency of targets.
A14 CTLs engaging $CD4^+$ T-cells pulsed with the indicated doses of SL9 peptide in collagen were imaged for 10 hr (E:T ratio 1:2). Outcomes for each target in view upon initiation of CTL-target imaging are expressed. Data shown from 1 representative of 5 independent experiments.

4.4 PRIMARY HIV-SPECIFIC CTL DYNAMICS ARE QUALITATIVELY SIMILAR TO CTL CLONES

Since it cannot be assumed that CTL clones retain all features of primary $CD8^+$ T-cells, we also assessed the dynamics of bulk primary CTLs derived from a patient who spontaneously controlled HIV infection. As expected (Migueles et al., 2008; Saez-Cirion et al., 2007), $CD8^+$ T-cells had little lytic activity immediately ex vivo (data not shown), and thus were primed with a Gag/Pol/Nef/Env peptide pool for a limited period of 12 days (**Figure 4.16a**) at which time antigen-specific killing activity was detected by ^{51}Cr release (**Figure 4.16b**). These primary CTLs engaged and killed autologous $CD4^+$ T-cell targets pulsed with pooled HIV peptides with the same 4 characteristic engagement types observed with CTL clones (**Figure 4.17**). Furthermore, in a manner similar to the clones, primary CTLs exhibited rapid arrest of CTL migration and rapid target death kinetics followed by long-lived engagements with killed targets (**Figure 4.18a-c, Video 8**). Thus, after a brief period of re-exposure to antigen, primary HIV-specific CTLs share the same dynamic program of killing and sustained motility arrest observed with the HIV-specific A14 and E501 CTL clones.

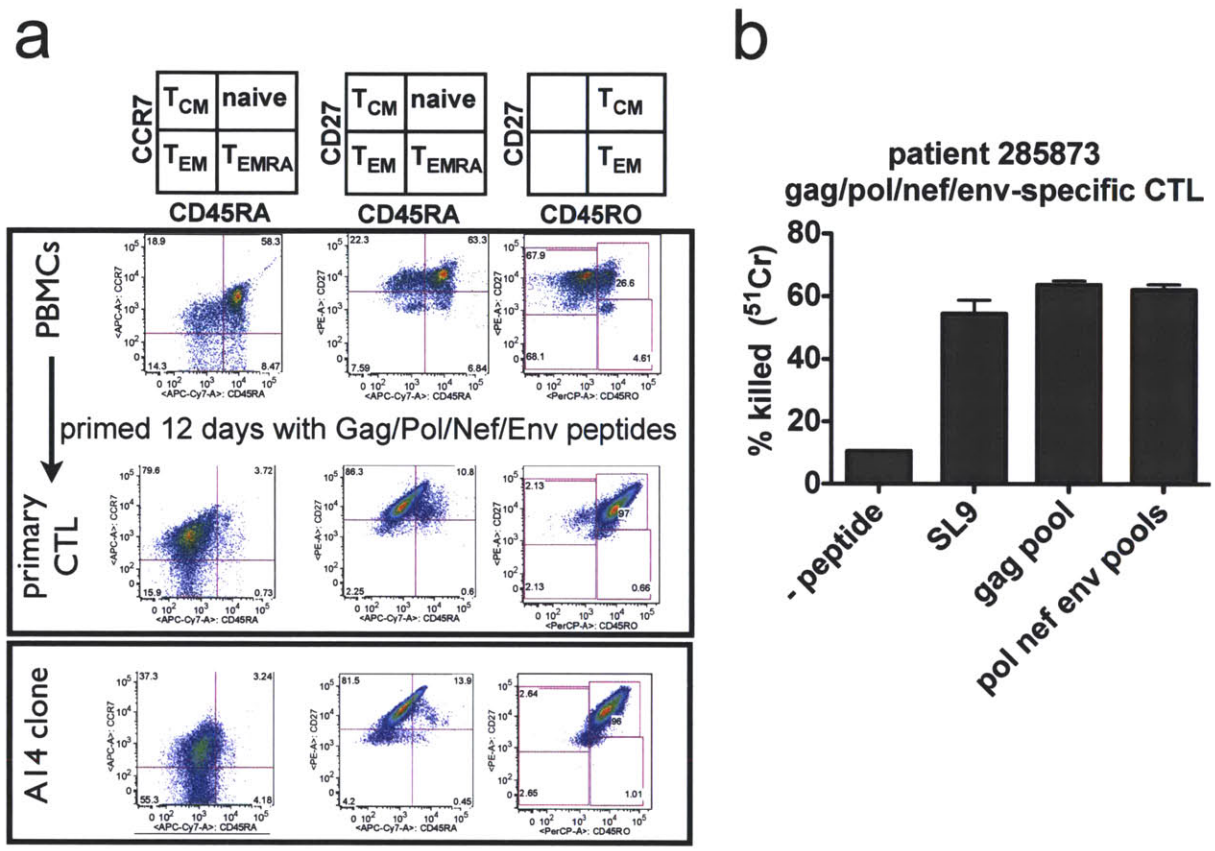

Figure 4.16. Primary HIV-specific CTLs exhibit lytic activity *ex vivo* following a brief re-exposure to antigen.

$CD8^+$ T cells purified from elite controller PBMCs were activated for 12 days with HLA-matched targets bearing gag, pol, env, and nef peptides. (**a**) Primary, activated HIV-specific CTLs were stained with memory markers and analyzed by FACS. Scatter plots are gated on $CD8^+$ cells which represented ~90% of total cells. (**b**) CTLs were mixed with autologous targets bearing SL9 peptide, pooled gag peptides, or pooled env, nef, pol peptides in a traditional ^{51}Cr release assay at an E:T ratio of 7:1. Shown is one representative of 3 independent experiments. Bars indicate mean ± SEM.

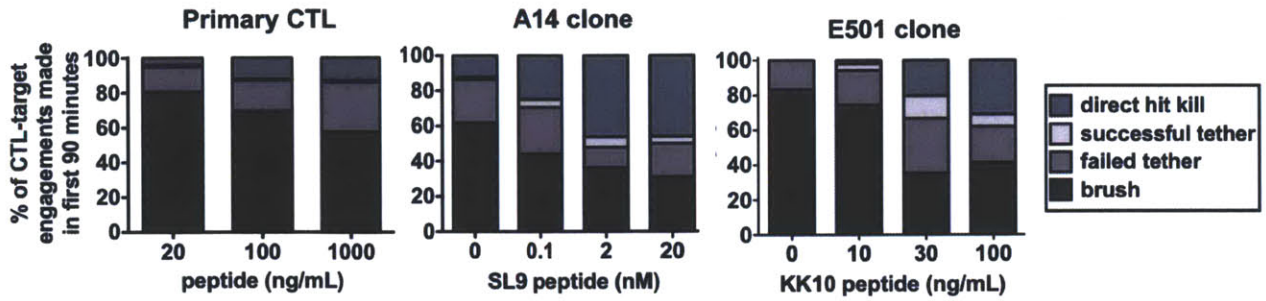

Figure 4.17. Primary HIV-specific CTLs exhibit characteristic dynamics qualitatively similar to CTL clones.

Primary CTLs engaged and killed autologous targets pulsed with Gag/Pol/Nef/Env peptide pools (20, 100, and 1000 ng/mL of each peptide) in collagen matrices during 90 minutes of imaging. CTL-target engagement dynamics were observed and exhibited the four characteristic engagement types at the indicated frequencies. For comparison, data is shown for clones A14 and E501 in response to targets pulsed with the indicated concentrations of cognate antigen.

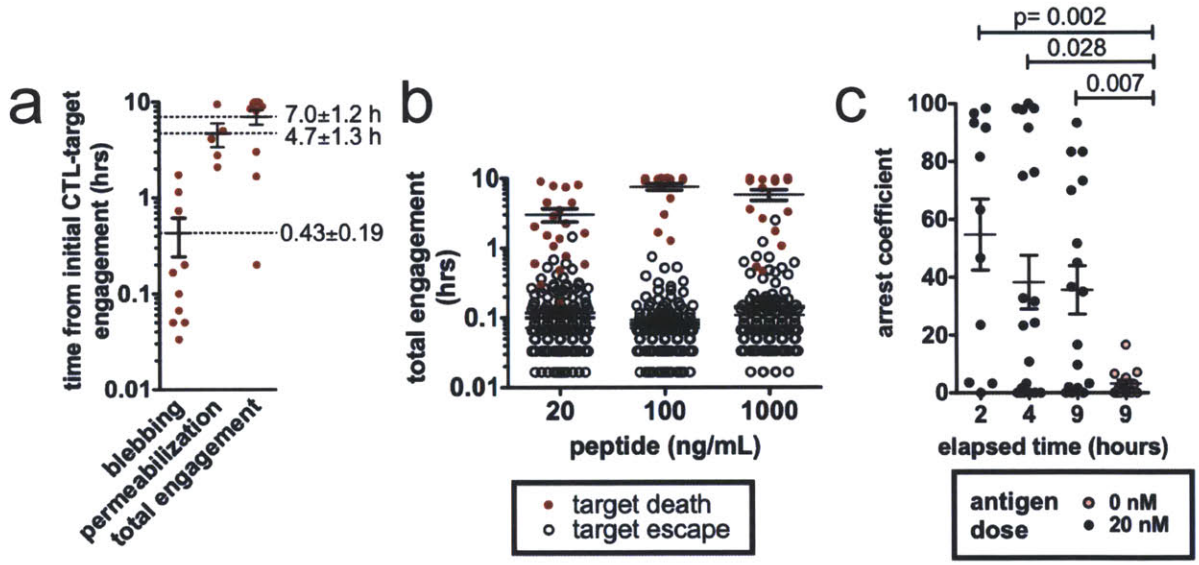

Figure 4.18. Primary HIV-specific CTLs exhibit a dynamic program of killing and sustained arrest similar to CTL clones.

CTLs engaged and killed autologous targets pulsed with Gag/Pol/Nef/Env peptide pools (20, 100, and 1000 ng/mL of each peptide) in collagen matrices during 10 hr of imaging. (**a**) Kinetics of target death and total duration of CTL-target engagement. (**b**) Duration of individual CTL-target engagements (leading to target death or target escape). (**c**) CTL arrest coefficients were calculated from 1 hr intervals after 2, 4, or 9 hr of co-culture as they encountered targets pulsed with the indicated peptide doses. Bars indicate mean ± SEM.

4.4 PRIMARY HIV-INFECTED CD4$^+$ T-CELLS ELICIT A CTL PROGRAM SIMILAR TO PEPTIDE-PULSED TARGETS

Since HIV-driven mechanisms for evading CTLs are well established (Collins et al., 1998; Schwartz et al., 1996), we next tested whether HIV-infected targets were recognized by CTLs with similar dynamics as observed with peptide-pulsed target cells. HIV-infected primary CD4$^+$ target cells were purified by flow sorting GFP$^+$ cells following 3 days of infection with an NL4-3-GFP virus expressing the E501 CTL target gag epitope. As previously reported (Nobile et al., 2010), ~1/3 of infected cells retained migration speeds comparable to uninfected cells (**Figure 4.19**). E501 CTLs engaged and killed motile HLA-matched GFP$^+$ infected targets by

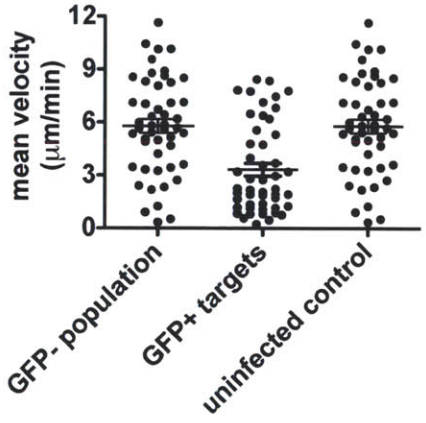

Figure 4.19. Motility of HIV-infected CD4$^+$ T cells.
CD4$^+$ T cell targets were infected with NL4-3 IRES-GFP virus and a pure population of infected cells was obtained by FACS sorting of GFP$^+$ cells. The sorted GFP$^-$ cells, GFP$^+$ infected cells, and cells from a control uninfected culture were imaged in collagen matrix. Mean velocities for individual CD4$^+$ cells tracked for one hour are shown. Shown is one representative of 3 independent experiments. Bars indicate mean ± SEM.

direct hits or successful tethers, but did not kill GFP$^-$ uninfected cells, and target killing was associated with rapid motility arrest (**Figure 4.20**, **Video 9**, first and second segments). CTLs killed targets with a mean time of only 15 min to blebbing and 92 min to permeabilization, but engagement with targets was prolonged (**Figure 4.21**, mean of 3.0 ± 0.4 hrs), and motility arrest persisted for >8 hours (**Figure 4.22**). Thus, HIV-infected cells presenting endogenously-processed antigen elicit an immediate and prolonged CTL stop signal during killing, in qualitative agreement with the findings for peptide-pulsed targets.

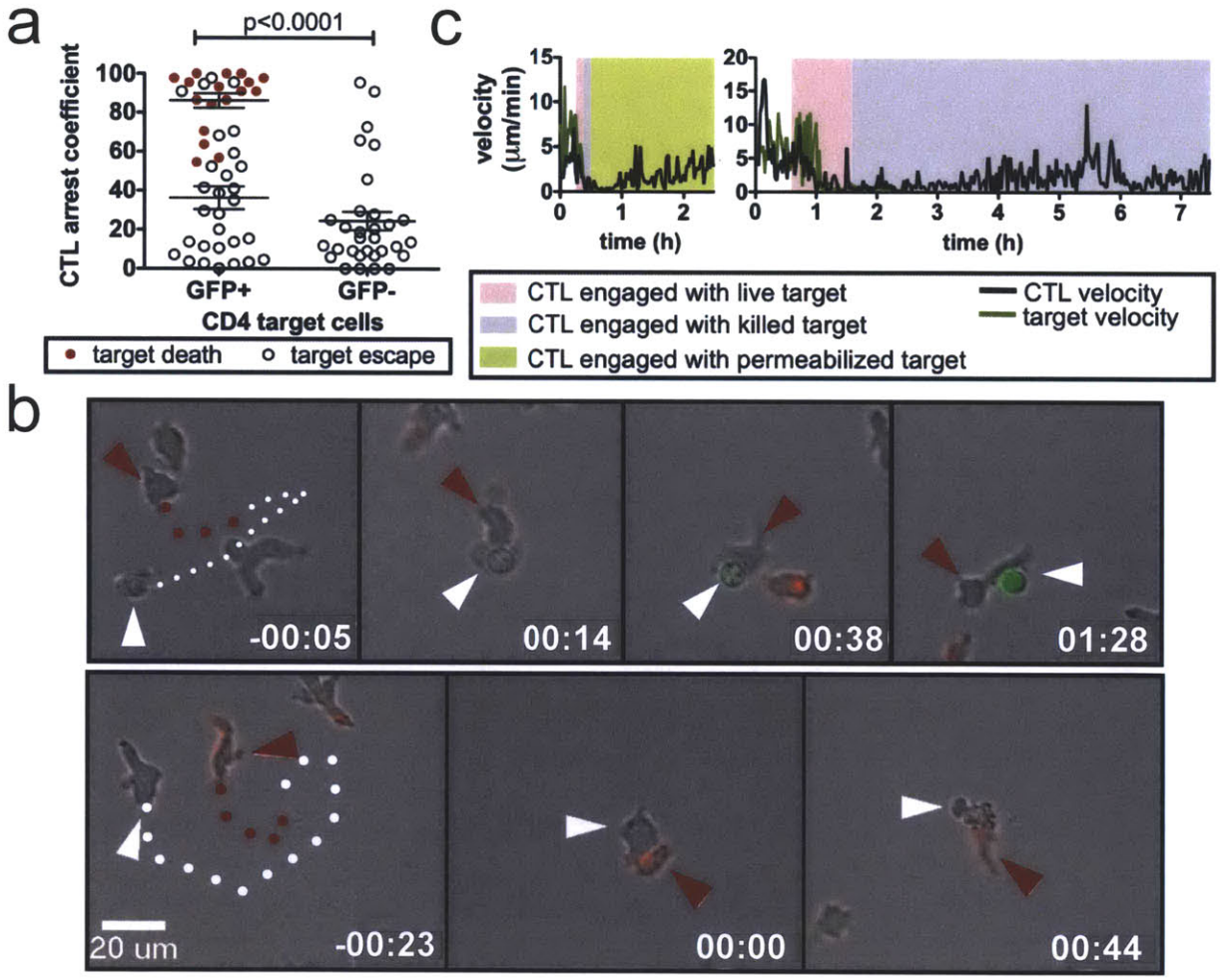

Figure 4.20. HIV-infected target cells elicit CTL killing with similar dynamics to peptide-pulsed targets.

E501 CTLs were imaged in collagen interacting with NL4-3 IRES-GFP HIV-infected CD4$^+$ targets. (**a**) The infected cell population was sorted into GFP$^-$ and GFP$^+$ fractions, respectively,

and imaged in collagen with E501 CTLs (E:T ratio 1:2). CTL arrest coefficients were determined for engagements leading to target death or escape during hours 1-2 of imaging. (**b, c**) E501 CTLs were imaged in collagen at an E:T of 1:2 on day 3 post-infection when 30% of targets were $p24^+$ by flow cytometry. (**b**) Representative time-lapse sequences showing two typical CTLs killing infected targets; elapsed times shown in hr:min. (**c**) Velocities of CTL and target over time for examples shown in (**b**). Data shown from 1 representative of 3 independent experiments. Bars indicate mean ± SEM.

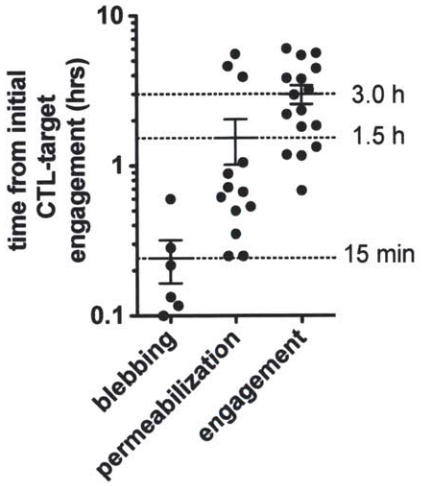

Figure 4.21. HIV-infected target cells elicit CTL killing with similar kinetics to peptide-pulsed targets.
E501 CTLs were imaged in collagen interacting with NL4-3 IRES-GFP HIV-infected $CD4^+$ targets. Kinetics of CTL-target engagements leading to target death were analyzed.

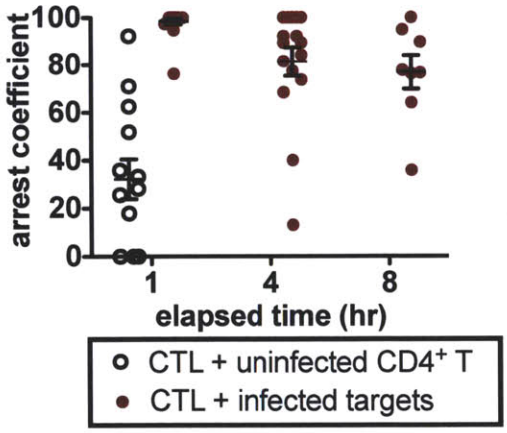

Figure 4.22. Durable CTL migration arrest upon lysis of physiological targets.
E501 CTLs were imaged in collagen interacting with NL4-3 IRES-GFP HIV-infected $CD4^+$ targets or uninfected control cells. CTL arrest coefficients were calculated from 1 hr intervals after 1, 4, or 8 hr of co-culture. Bars indicate mean ± SEM.

4.5 CTLs RAPIDLY TRANSITION TO SUSTAINED NON-LYTIC EFFECTOR SECRETION DURING PROLONGED ARREST

The low frequency of serial killing following initial target lysis observed with peptide-pulsed targets was unexpected, given that A14 CTLs effectively inhibited viral replication in co-cultures with HIV-infected $CD4^+$ T-cells in ECM (**Figure 4.23a**). Since viral suppression is an aggregate measure of lytic and non-lytic CTL function, we hypothesized that prolonged CTL arrest on dead targets with continued calcium signaling (**Figure 4.3b**) reflected TCR signal accumulation in support of a transition from early lysis to sustained anti-viral factor secretion. To determine whether effector secretion coincided temporally with CTL arrest and initiation of killing, we measured the kinetics of cytokine/chemokine secretion in collagen. At an antigen dose (20 nM SL9) where >95% of A14 CTLs engaged a target and arrested within 30 min of co-culture (**Figure 4.23b**), cytokine and chemokine secretion was detected after 2 hr, as previously reported for CTLs in liquid cultures (Purbhoo et al., 2001). However, secretion was strikingly sustained for at least 12 hr while CTLs remained arrested (**Figure 4.23c**). Primary HIV-specific CTLs also secreted cytokine and chemokine within 6 hr in response to peptide-pulsed, autologous targets in liquid and in collagen (**Figure 4.23d** and data not shown).

Finally, we directly examined the role for TCR signal accumulation in supporting sustained non-lytic secretory function. Under conditions of low avidity (but equivalent doses/ densities of antigen) A14 CTLs failed to achieve maximal upregulation of secreted factors (**Figure 4.24a**). Furthermore, under conditions where A14 CTL killing was executed with near-perfect efficiency and all CTLs were committed to targets within 1 hour, sustained secretion was uncoupled from maximal killing by addition of dasatinib, an inhibitor of TCR signaling, after 1 or 5 hours of coculture (**Figure 4.24b**). Taken together, these data indicate that CTL clones

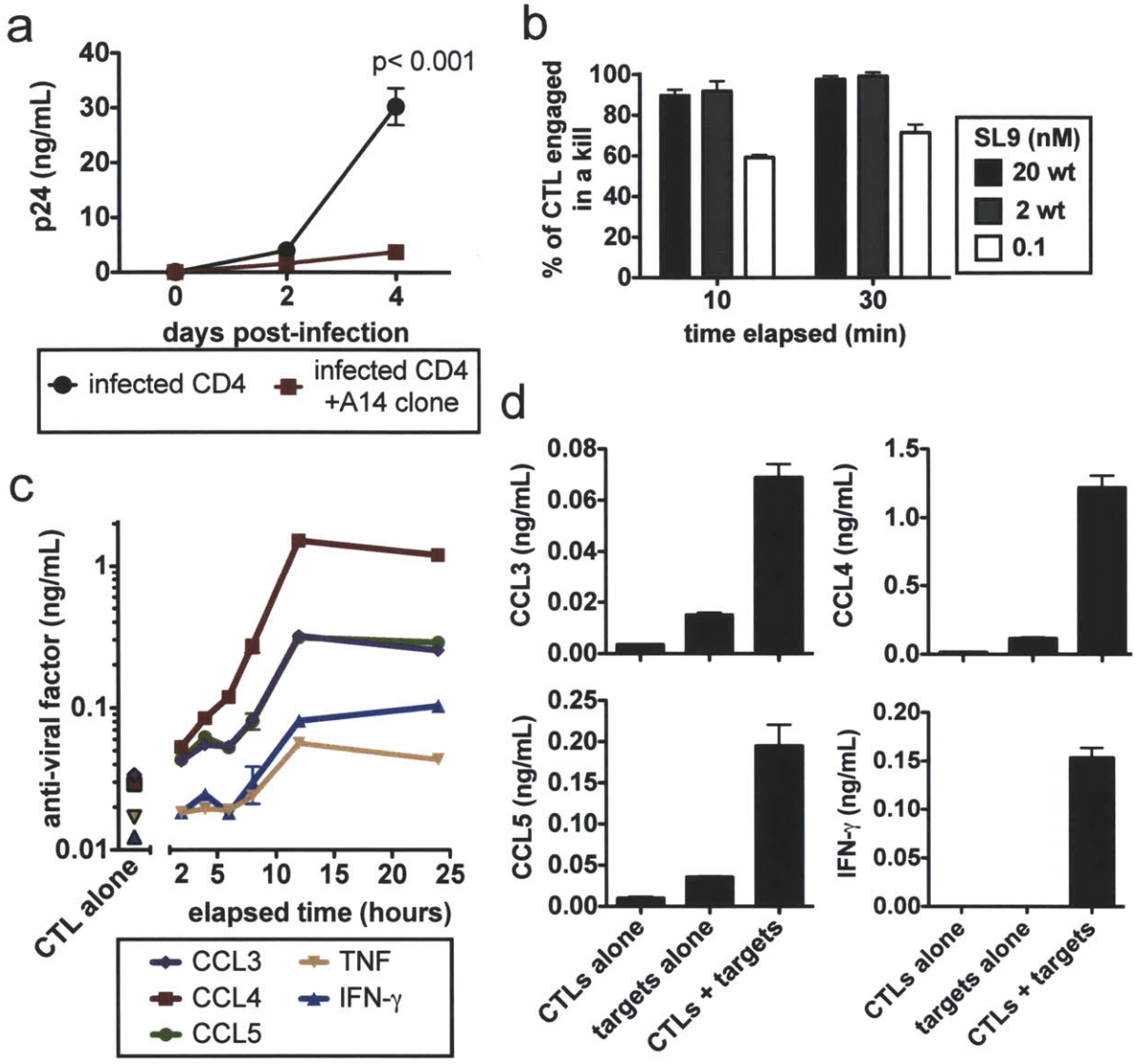

Figure 4.23. CTLs rapidly transition from killing to sustained non-lytic effector secretion during prolonged arrest.

(**a**) CD4$^+$ T cells infected with JR-CSF HIV-1 were cultured in collagen gels with or without CTL clone A14 (E:T 1:1) in triplicate, and HIV replication was assessed by p24 ELISA. Data from one representative of 3 independent experiments. Bars indicate mean ± SEM. (**b**) A14 CTLs were co-cultured with antigen-pulsed CD4$^+$ T cell targets in collagen (E:T ratio 1:2) and imaged. The percentage of CTLs engaged with a target was assessed at the indicated times. (**c, d**) Concentrations of secreted cytokines/chemokines supernatants from co-cultures. (**c**) A14 CTLs and CD4$^+$ target cells pulsed with 20 nM SL9 were cultured in collagen gels for 2, 4, 6, 8, 12 and 24 hrs. Data shown from 1 representative of 3 independent experiments. Bars indicate mean ± SEM. (**d**) Primary HIV-specific CTLs were cultured with autologous targets pulsed with gag/env/nef/pol peptide pools (each unique peptide at 20 ng/mL) in liquid for 6 hrs. Bars indicate mean ± SEM.

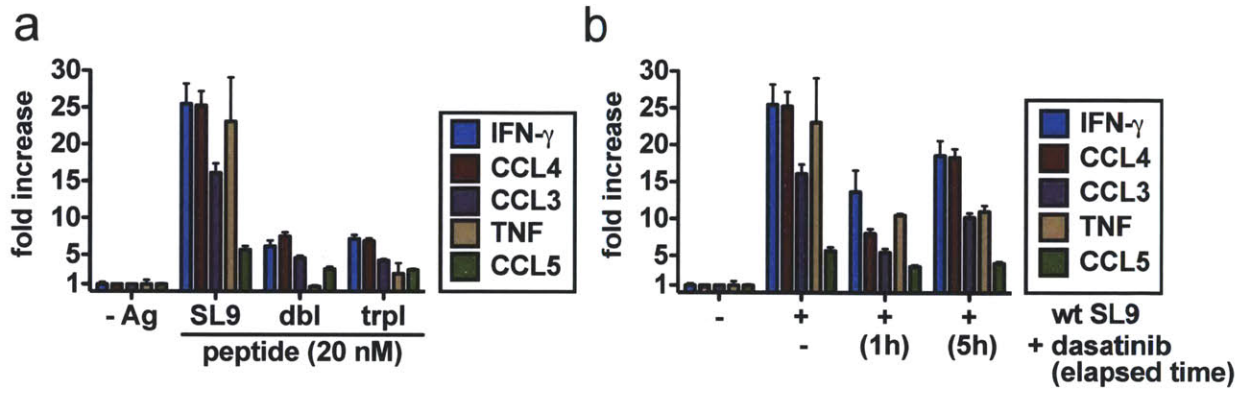

Figure 4.24. Sustained non-lytic effector secretion is dependent on strong, prolonged TCR signals accumulated after target death.
A14 CTLs were co-cultured in collagen gels with HLA-matched $CD4^+$ target cells pulsed with the indicated peptides (20 nM). Secreted cytokines and chemokines were measured in supernatants collected after 24 hrs of co-culture. Expressed as fold increase over secretion in response to targets without cognate antigen. (**a**) Secretion under conditions of high (wt SL9) or lower functional avidity (double, triple mutant SL9). (**b**) Secretion under conditions of high (20 nM wt SL9) functional avidity with or without addition of an inhibitor of TCR-proximal signaling (50 μM dasatinib) after 1 or 5 hrs of co-culture.

capable of suppressing viral replication *in vitro* coordinate their lytic and non-lytic effector functions spatiotemporally in ECM; high avidity CTLs transition from rapid migration and an efficient initial kill to durable arrest on dead targets coincident with sustained upregulation of anti-viral effector molecule secretion; prolonged TCR signal accumulation is required for maximal upregulation of cytokines and chemokines; and low avidity CTL-target interactions fail not only to support high killing efficiency but also fail to support maximal secretory function.

4.6 CONCLUSIONS

In this thesis we developed a new assay for monitoring cell migration dynamics and cell-mediated killing over many hours. Much is known about CTL function: CTLs initiate TCR signaling and undergo migration arrest in response to antigen-bearing targets, and these TCR signals induce multiple functions including delivery of a lethal hit to targets and upregulation of

a variety of secreted anti-viral factors. However, this work has revealed several important features of the CTL response by modulating TCR signal strength while simultaneously assessing short-term and long-term CTL function and CTL migration dynamics within a model system. First, target migration directly reduces the efficiency of CTL killing on the single-cell level. Secondly, while it is well known that CTLs exhibit rapid delivery of a lethal hit upon target encounter (Jenkins et al., 2009b; Stinchcombe et al., 2001; Wiedemann et al., 2006), and many researchers have postulated that CTLs may rapidly kill many targets in a "serial killing" fashion (Cerottini and Brunner, 1974; Isaaz et al., 1995; Poenie et al., 1987; Rothstein et al., 1978; Zagury et al., 1975), we report that in the context of ECM (where T-cell migration is governed by T-cell intrinsic stop and go signals) CTLs remain engaged with their initial killed target for many additional hours and do not rapidly kill numerous targets. Third, CTL secretion of anti-viral factors is dependent on sustained TCR signal accumulation during prolonged CTL engagement an initial killed target. Fourth, the prolonged TCR stop signal revealed by our continuous videomicroscopy approach indicates that lytic and non-lytic anti-viral effector functions are spatially coordinated within the precise microenvironment where antigen has been sensed. Fifth, high avidity antigen recognition is required for efficient CTL killing and CTL killing and arrest is a necessary prerequisite for induction of non-lytic CTL secretory function. Thus, we arrive at a more integrated model of CTL function that was previously understood in fractured facets.

CHAPTER 5. CONCLUSIONS AND FUTURE WORK

5.1 SUMMARY OF RESULTS

Here we analyzed the kinetics of CTL killing within a 3D surrogate of peripheral tissue extracellular matrix where both CTLs and target cells exhibited rapid random-walk migration. HIV-specific $CD8^+$ T-cells were subjected to continuous observation for periods of up to 24 hr, permitting quantitative analysis of long-term dynamics presently inaccessible *in vivo*. This approach revealed a new role for TCR avidity in regulating the function of CTLs: High-avidity CTLs were capable of near-perfect efficacy in capturing and killing migrating targets on first contact, while target cell motility facilitated escape from CTLs under conditions of weak antigen recognition (low antigen dose or low-avidity TCR/peptide-MHC interactions). Second, we found that CTLs coordinated effector functions in two phases: a rapid "commitment phase" (migrating, engaging, and killing of initial targets), followed by a prolonged "secretory phase" (durable migration arrest and TCR signaling without further killing, accompanied by sustained effector molecule secretion).

Successful CTL engagement of motile target cells within ECM was accompanied by an initial cascade of prototypical TCR-mediated events previously characterized in liquid suspensions (Dustin et al., 1997; Purbhoo et al., 2001; Wiedemann et al., 2006): calcium signaling (within seconds) and motility arrest (within minutes); followed by signatures of target death, membrane blebbing (as early as 2 min) and permeabilization (as early as 5 min). However, we found that in ECM where migration/arrest is CTL-intrinsic, CTLs did not immediately detach from dead targets upon lethal hit delivery, instead remaining arrested (frequently >10 hr), largely failing to engage and kill subsequent passing targets. These data are consistent with short-term *in*

vivo studies where intravital imaging durations are limited (30-60 min), but which report slow rates of killing (Breart et al., 2008; Coppieters et al., 2011) and direct observation of sustained CTL-dead target engagement and CTL arrest (Boissonnas et al., 2007; Mempel et al., 2006; Mrass et al., 2006). The present *in vitro* model allowed the temporal window of observation to be extended by >10-fold, revealing a transition from rapid killing to prolonged CTL arrest, during which CTLs continued to accumulate TCR signals, coincident with the induction of sustained secretion of effector cytokines and chemokines (at least 12 hr). Thus, strong TCR stimulation drives a program of spatially coordinated, multidimensional (i.e., combined lytic and secretory) CTL function.

5.2 DISCUSSION

Multiple dimensions of CTL activity have been correlated with control of HIV *in vivo*: these include high lytic capacity (Migueles et al., 2008), functional avidity (Almeida et al., 2007), β-chemokine expression (Cocchi et al., 2000; Dolan et al., 2007), polyfunctionality (i.e. lytic degranulation and non-lytic anti-viral effector molecule production) (Betts et al., 2006; Genesca et al., 2008), and proliferative capacity (Almeida et al., 2007; Migueles et al., 2008). CTL functions are induced according to a hierarchy of TCR signaling thresholds, with increasing TCR signals driving increased polyfunctionality (Almeida et al., 2009; Valitutti et al., 1996). Net TCR signals are integrated over time (Celli et al., 2005) and are dictated not only by the quantity and quality of antigen presented by the target cell but also by the duration of T-cell contact with the target. Notably, we found that the duration of CTL-target engagement is not pre-programmed but rather controlled by TCR signal strength, and that TCR signal accumulation can continue post-target-death. Thus, strong early TCR engagement initiates a positive feedback loop by triggering prolonged arrest of the CTL in contact with antigen, leading to greater net TCR signal

accumulation that in turn promotes greater CTL polyfunctionality. By contrast, while weak TCR signaling may mediate target death, it results in poor effector function since TCR signal accumulation is prematurely cut short by abandonment of the dead target.

These results must be interpreted within the limitations of our reductionist approach. This model system of CTLs and target cells eliminates many variables present *in vivo*, and clearly many additional immune cells and mechanisms contribute to the spread and/or control of virus *in vivo* (McMichael et al., 2010). However, this methodology permitted detailed analysis of human CTL killing dynamics presently inaccessible *in vivo*, under conditions where the phenotypic and functional characteristics of targets and killer cells were well defined. Only two CTL clones and freshly-primed CTLs from one patient were examined, but all gave concordant results. Other tissue-resident cells or soluble factors could be present in tissues that could influence cell motility and/or CTL function, but notably, addition of potent motility-driving chemokines such as CCL21 did not alter the sustained stop signal behavior of CTLs here (data not shown).

Together, our findings lead us to propose a two-phase model for control of infection by individual CTLs exhibiting cooperative behavior on the population level (**Figure 5.1**): On detecting antigen, rather than attempting to control infection individually through serial lytic hits, high-avidity CTLs efficiently engage and kill initial targets (commitment phase) followed by a rapid transition to bathe the local microenvironment with inflammatory factors (secretory phase). In this scenario, sustained secretion of β-chemokines may rapidly shift the local E:T ratio, by blocking infection of new targets and recruiting additional "ready-to-kill" CTL effectors into the tissue; sustained TCR signaling may also drive proliferation of CTLs post-kill. Conversely, low-avidity CTLs will exhibit multifaceted failure: motile targets will escape inefficient engagement,

triggering prolonged arrest of the CTL in contact with antigen, leading to greater net TCR signal accumulation that in turn promotes greater CTL polyfunctionality. By contrast, while weak TCR signaling may mediate target death, it results in poor effector function since TCR signal accumulation is prematurely cut short by abandonment of the dead target.

These results must be interpreted within the limitations of our reductionist approach. This model system of CTLs and target cells eliminates many variables present *in vivo*, and clearly many additional immune cells and mechanisms contribute to the spread and/or control of virus *in vivo* (McMichael et al., 2010). However, this methodology permitted detailed analysis of human CTL killing dynamics presently inaccessible *in vivo*, under conditions where the phenotypic and functional characteristics of targets and killer cells were well defined. Only two CTL clones and freshly-primed CTLs from one patient were examined, but all gave concordant results. Other tissue-resident cells or soluble factors could be present in tissues that could influence cell motility and/or CTL function, but notably, addition of potent motility-driving chemokines such as CCL21 did not alter the sustained stop signal behavior of CTLs here (data not shown).

Together, our findings lead us to propose a two-phase model for control of infection by individual CTLs exhibiting cooperative behavior on the population level (**Figure 5.1**): On detecting antigen, rather than attempting to control infection individually through serial lytic hits, high-avidity CTLs efficiently engage and kill initial targets (commitment phase) followed by a rapid transition to bathe the local microenvironment with inflammatory factors (secretory phase). In this scenario, sustained secretion of β-chemokines may rapidly shift the local E:T ratio, by blocking infection of new targets and recruiting additional "ready-to-kill" CTL effectors into the tissue; sustained TCR signaling may also drive proliferation of CTLs post-kill. Conversely, low-

avidity CTLs will exhibit multifaceted failure: motile targets will escape inefficient engagement, permitting viral replication and spread, while upon killing a target, weak TCR signaling and secretion of low quantities of β-chemokines insufficient for blocking new infections might recruit additional $CD4^+$ cells to the tissue, thereby inadvertently promoting rapid viral replication (Li et al., 2009). This mechanism for spatiotemporal coordination of anti-viral effector functions is dependent on CTL killing efficiency and highlights a new role for TCR avidity in tissue where CTLs and targets are motile. Thus, a successful HIV vaccine employing $CD8^+$ T-cells will need to induce high-avidity CTLs, which can mount a cooperative and multidimensional response for efficient elimination of migrating infected cells prior to overwhelming virus dissemination.

5.3 CONCLUSIONS AND MODEL

Together, our findings lead us to propose a two-phase model for cooperative control of infection by CTL populations (**Figure 5.1**): On detecting antigen, rather than attempting to control infection individually through serial lytic hits, high-avidity CTLs efficiently engage and kill initial targets (commitment phase) followed by a rapid transition to bathe the local microenvironment with inflammatory factors (secretory phase). In this scenario, sustained secretion of β-chemokines may rapidly shift the local E:T ratio, by blocking infection of new targets and recruiting additional "ready-to-kill" CTL effectors into the tissue; sustained TCR signaling may also drive proliferation of CTLs post-kill. Conversely, low-avidity CTLs will exhibit multifaceted failure: motile targets will escape inefficient engagement, permitting viral replication and spread, while upon killing a target, weak TCR signaling and secretion of low quantities of β-chemokines might recruit additional $CD4^+$ cells to the tissue without reaching

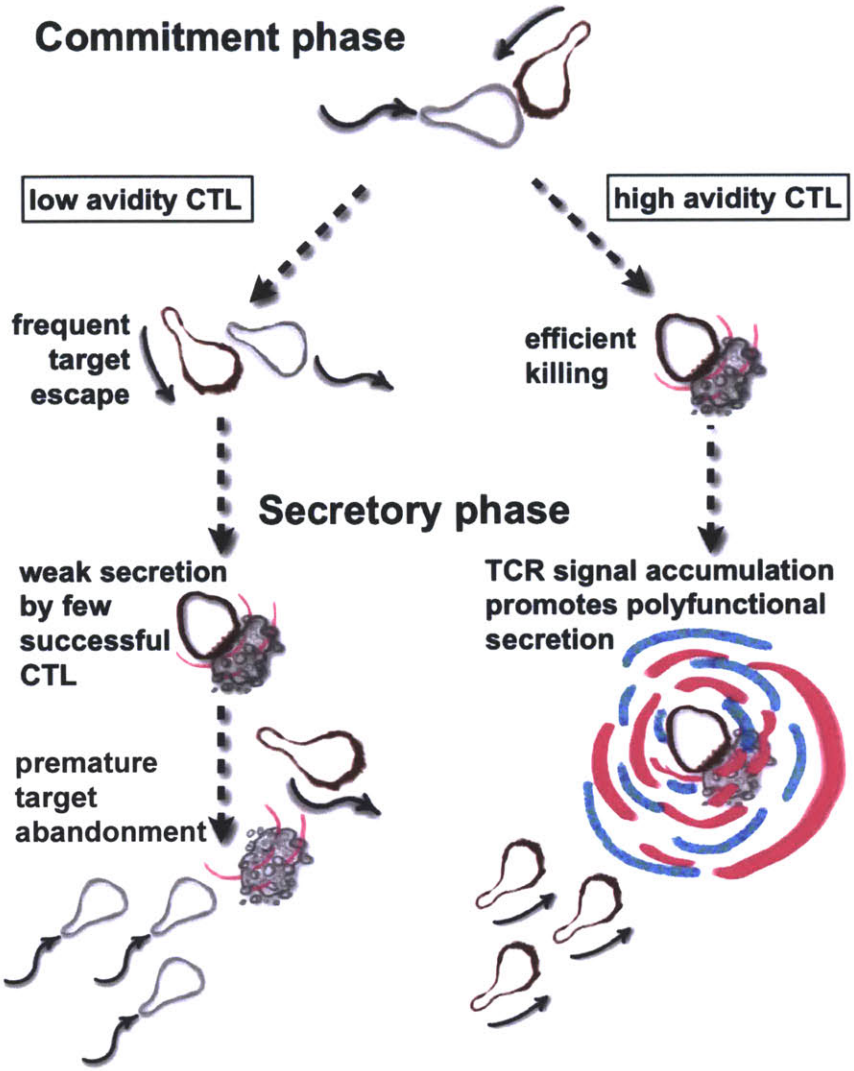

Figure 5.1. A model of effective anti-viral CTL function in a 3D environment.
High avidity CTLs efficiently kill motile targets and rapidly transition to a polyfunctional secretory phase which is driven by prolonged CTL-dead target engagements and TCR signal accumulation.

levels sufficient to block new infections, thereby inadvertently promoting rapid viral replication (Li et al., 2009a). CTL killing efficiency is a new parameter of single-cell CTL function in the context of ECM and rapid cellular migration. We highlight a new role for TCR avidity and killing efficiency in the development and spatiotemporal coordination of multidimensional anti-viral effector function. These results suggest that a successful HIV vaccine employing $CD8^+$ T-cells will need to induce high-avidity CTL in substantial numbers, which can coordinately eliminate migrating infected cells prior to overwhelming virus dissemination.

5.4 FUTURE WORK

This work has laid a strong foundation for the understanding of CTL dynamics and function, but has also prompted several additional questions. We hypothesize that the program of CTL dynamics and function described here is a general, CTL-intrinsic program and is likely utilized by CTLs specific for other disease related antigens. Thus it would be of great interest to examine the dynamics of CTLs taken from HIV^+ patients during the acute phase of HIV infection, or specific for rapidly resolved diseases such as flu or chicken-pox; chronic diseases such as CMV, hepatitis, and cancer; or autoimmune diseases such as diabetes. In light of our findings, it would be of interest to examine the effects of immunosuppressive receptors such as PD-1 and CTLA-4 on the dynamics of CTL-target engagement. These molecules not only play important roles in the induction of anergy in the context of HIV and cancer, but they are also reported to override TCR stop signals (Fife et al., 2009; Schneider et al., 2006) and might thus decrease the efficiency of CTL killing.

The CCR5 chemokine receptor is expressed on effector $CD8^+$ and $CD4^+$ T cells and directs their traffic into inflamed peripheral and mucosal tissues in response to the β-chemokines

CCL3, CCL4, CCL5 (Mora and von Andrian, 2006; Weninger et al., 2002). It also guides naive $CD8^+$ T cells to join T-DC couples during T-cell priming in lymph nodes (Castellino et al., 2006), enhances early T cell contacts with antigen presenting cells (Friedman et al., 2006), and generates costimulatory signals which contribute to TCR-dependent T cell activation (Hugues et al., 2007; Molon et al., 2005). Thus, it is intriguing that while CTLs can kill targets in 5-20 minutes (Stinchcombe et al., 2001), CTLs secrete an initial burst of preformed stores of β-chemokines with similarly rapid kinetics (Catalfamo et al., 2004; Purbhoo et al., 2001; Wagner et al., 1998). The primary and cloned HIV-specific CTLs examined here secrete β-chemokines within 20 minutes (data not shown) and exhibit upregulated secretion within 2 hours. The assay system developed here could be utilized to examine what role these early bursts of β-chemokines play in CTL-target engagement efficiency. In one of our very first experiments we examined if the E501 CTL response affected the antigen-independent dynamics of the A14 CTLs and we found no significant effects on A14 velocities or arrest coefficient (**Figure 3.2b, c**). However, given the integrated model of CTL dynamics and function (**Figure 5.1**), and given our ability to monitor multiple populations of CTLs labeled with unique fluorophore-CTXB tracers (**Figure 3.2a**) it would be very interesting to examine the efficiency of low avidity E501 CTL killing in the presence of the high avidity A14 CTL response. One might predict that E501 CTL killing efficiency would be enhanced.

Finally, specific molecular mechanisms of CTL killing were outside the scope of this thesis, but the videomicroscopy data revealed target deaths of at least three seemingly distinct morphologies, consistent with reports of FasL mediated apoptosis (blebbing with delayed or absent permeabilization), perforin and granzyme mediated apoptosis (blebbing followed by

partial permeabilization indicated by only dim nuclear staining that gets brighter over time), and complete and rapid target lysis mediated by high doses of perforin (target membrane expands rapidly like a balloon coincident with immediate, bright DNA staining) (Keefe et al., 2005; Thiery et al., 2011; Waterhouse et al., 2006). Given recent reports on unique roles for distinct mechanisms of CTL killing *in vivo* (Janssen et al., 2010; Meiraz et al., 2009; Shanker et al., 2009), it might be desirable to use the videomicroscopy approach developed here to probe these mechanisms *in vitro*.

SUPPLEMENTARY VIDEOS

Supplementary Video 1. Target cell motility within collagen gels vs convection within traditional liquid culture.
$CD4^+$ T cells were imaged within 3D ECM (left panel) and in liquid culture (right panel). Elapsed time shown in min:sec; scale bar 20 μm.

Supplementary Video 2. CTL and target cells migrate within 3D ECM and CTL killing is not observed in the absence of cognate antigen.
A control culture containing primary HIV-specific CTL from an HIV^+ patient and autologous $CD4^+$ T cells (not pulsed with any peptides) was imaged within 3D ECM. CTL were stained with CTXB (red) and targets were unlabeled. Dead cells are visualized with sytox green. Elapsed time shown in hr:min; scale bar 20 μm.

Supplementary Video 3. Recognition, engagement and killing of target cells in ECM.
A14 CTLs were co-cultured in ECM with HLA-matched $CD4^+$ T cell targets pulsed with SL9 peptide (2 nM). (**video segment 1**) A successful CTL-target engagement characteristic of a "direct hit kill," and (**video segment 2**) a dramatic example of a "successful tether" followed by target death indicated by "ballooning" of the target cell membrane. The following cues are included: CTL, red arrow; target, white arrow; elapsed time shown in hr:min; scale bar 20 μm. Target permeabilization is visualized *in situ* with sytox green.

Supplementary Video 4. CTL exhibits prolonged TCR signaling following a direct hit kill.
A14 CTLs were double labeled with CTXB and the ratiometric calcium-sensing dye, FURA-2AM prior to loading in ECM. An A14 CTL engages and kills an HLA-matched $CD4^+$ T cell target pulsed with SL9 peptide (2 nM). The top video panel is a brightfield/CTXB fluorescence overlay of CTL-target engagement dynamics. TCR-dependent calcium signaling is represented in pseudocolor video (bottom video panel) and is quantitatively expressed over time as a normalized Fura ratio (right panel). On the x-axis CTL engagement with the live target is indicated in pink, prolonged CTL engagement with the killed target is indicated in gray. The following video cues are included: CTL, red arrow; target, white arrow; elapsed time shown in min; scale bar 20 μm.

Supplementary Video 5. Failed CTL encounter with migrating target in ECM leads to target escape.
A14 CTLs were co-cultured in ECM with HLA-matched $CD4^+$ T cell targets pulsed with SL9 peptide (2 nM). Shown are characteristic examples of targets escaping CTLs following a "failed tether" (**video segment 1**) and a "brush" (**video segment 2**). The following cues are included: CTL, red arrow; target, white arrow; scale bar 20 μm, elapsed time shown in min and hr:min, respectively.

Supplementary Video 6. CTL exhibits weak TCR signaling during a failed tether.
A14 CTLs were double labeled with CTXB and the ratiometric calcium-sensing dye, FURA-2AM prior to loading in ECM. An A14 CTL engages but fails to kill an HLA-matched

$CD4^+$ T cell target pulsed with SL9 peptide (2 nM). The left video panel is a brightfield/CTXB fluorescence overlay of CTL-target engagement dynamics. TCR-dependent calcium signaling is represented in pseudocolor video (right panel) and is quantitatively expressed over time as a normalized Fura ratio (bottom panel). On the x-axis CTL engagement with the live target is indicated in pink. The following video cues are included: CTL, red arrow; target, white arrow; elapsed time shown in min; scale bar 20 μm.

Supplementary Video 7. Kill-experienced CTLs arrest for hours and fail to kill subsequent targets.

A14 CTLs were co-cultured in ECM with HLA-matched $CD4^+$ T cell targets pulsed with the indicated concentrations of cognate peptide. **(video segment 1)** An A14 CTL was observed to kill a target (20 nM SL9) followed by prolonged engagement with the killed target and durable migration arrest after CTL disengagement. The permeabilized target is marked with sytox green. **(video segment 2).** An efficient first kill is quickly followed by inefficient recognition and engagement of subsequent targets (2 nM SL9). **(video segment 3)** An A14 CTL engages, kills and permeabilizes an initial target (2 nM SL9). While still arrested and engaged with the initial killed target, the CTL catches and kills a subsequent target. After "serially killing" two targets, this CTL remained arrested and engaged with the killed targets, permitting escape of three additional targets observed to run over the CTL. Target permeabilization is visualized with sytox green. The following cues are included: CTL, red arrow; target, white arrow; elapsed time shown in hr:min; scale bar 20 μm.

Supplementary Video 8. Primary CTL engage targets with dynamics similar to those observed for clones.

Primary, polyclonal HIV-specific CTLs from elite controller 285873 were primed with targets bearing overlapping 18-mer peptide pools covering the full sequences of Gag, Pol, Nef, and Env. On day 14 the polyclonal CTLs were labeled with CTXB and seeded in 3D ECM with autologous $CD4^+$ T cell targets pulsed with the same peptide pools (100 ng/mL). **(video segment 1)** A primary CTL commits a direct hit kill. Target permeabilization is visualized with sytox green. **(video segment 2)** A primary CTL exhibits a failed tether, followed by target escape. The following cues are included: CTL, red arrow; target, white arrow; scale bar 20 μm. Elapsed time shown in hr:min.

Supplementary Video 9. Primary HIV-infected $CD4^+$ T-cells elicit a CTL program similar to peptide-pulsed targets.

E501 CTLs were co-cultured with HLA-matched $CD4^+$ T cell targets infected with NL4-3 HIV virus. CTLs recognize physiologic antigen densities, engaging and killing HIV-infected targets. **(video segment 1)** CTL-target engagement is followed by target death indicated by "blebbing" of the target cell membrane and prolonged CTL arrest and contact with killed target. **(video segment 2)** A successful tether is followed by target death indicated by "blebbing" of the target cell membrane. The following cues are included: CTL, red arrow; target, white arrow; elapsed time shown in hr:min; scale bar 20 μm.

5.5 RESEARCH PUBLICATIONS AND CONFERENCE PRESENTATIONS

5.5.1 Publications

[1] **Hottelet Foley M**, Forcier T, McAndrew E, Juelg B, Walker BD, and Irvine DJ, "High avidity CTLs coordinate temporally uncoupled lytic and effector functions with a TCR-dependent stop signal", manuscript in preparation (2012).

5.5.2 Conference Presentations

[1] **Hottelet Foley M**, Forcier T, McAndrew E, Juelg B, Walker BD, and Irvine DJ, "Time-lapse videomicroscopy of HIV-specific CTLs: Effects of cell motility and TCR avidity on target engagement and killing." *Protection from HIV: Targeted Intervention Strategies (X8), Keystone Symposia*, Whistler, B.C. March 20-25, 2011.

REFERENCES

Almeida, J.R., Price, D.A., Papagno, L., Arkoub, Z.A., Sauce, D., Bornstein, E., Asher, T.E., Samri, A., Schnuriger, A., Theodorou, I., *et al.* (2007). Superior control of HIV-1 replication by CD8(+) T cells is reflected by their avidity, polyfunctionality, and clonal turnover. Journal of Experimental Medicine *204*, 2473-2485.

Almeida, J.R., Sauce, D., Price, D.A., Papagno, L., Shin, S.Y., Moris, A., Larsen, M., Pancino, G., Douek, D.C., Autran, B., *et al.* (2009). Antigen sensitivity is a major determinant of CD8(+) T-cell polyfunctionality and HIV-suppressive activity. Blood *113*, 6351-6360.

Ando, K., Hiroishi, K., Kaneko, T., Moriyama, T., Muto, Y., Kayagaki, N., Yagita, H., Okumura, K., and Imawari, M. (1997). Perforin, Fas/Fas ligand, and TNF-alpha pathways as specific and bystander killing mechanisms of hepatitis C virus-specific human CTL. J Immunol *158*, 5283-5291.

Andrade, F. (2010). Non-cytotoxic antiviral activities of granzymes in the context of the immune antiviral state. Immunol Rev *235*, 128-146.

Asquith, B., Mosley, A.J., Barfield, A., Marshall, S.E., Heaps, A., Goon, P., Hanon, E., Tanaka, Y., Taylor, G.P., and Bangham, C.R. (2005). A functional CD8+ cell assay reveals individual variation in CD8+ cell antiviral efficacy and explains differences in human T-lymphotropic virus type 1 proviral load. J Gen Virol *86*, 1515-1523.

Atkinson, E.A., and Bleackley, R.C. (1995). Mechanisms of lysis by cytotoxic T cells. Crit Rev Immunol *15*, 359-384.

Baker, B.M., Block, B.L., Rothchild, A.C., and Walker, B.D. (2009). Elite control of HIV infection: implications for vaccine design. Expert Opin Biol Th *9*, 55-69.

Bangham, C.R., and Osame, M. (2005). Cellular immune response to HTLV-1. Oncogene *24*, 6035-6046.

Barouch, D.H., O'Brien, K.L., Simmons, N.L., King, S.L., Abbink, P., Maxfield, L.F., Sun, Y.H., La Porte, A., Riggs, A.M., Lynch, D.M., *et al.* (2010). Mosaic HIV-1 vaccines expand the breadth and depth of cellular immune responses in rhesus monkeys. Nat Med *16*, 319-323.

Belyakov, I.M., Kuznetsov, V.A., Kelsall, B., Klinman, D., Moniuszko, M., Lemon, M., Markham, P.D., Pal, R., Clements, J.D., Lewis, M.G., *et al.* (2006). Impact of vaccine-induced mucosal high-avidity CD8+ CTLs in delay of AIDS viral dissemination from mucosa. Blood *107*, 3258-3264.

Bennett, M.S., Ng, H.L., Dagarag, M., Ali, A., and Yang, O.O. (2007). Epitope-dependent avidity thresholds for cytotoxic T-lymphocyte clearance of virus-infected cells. Journal of Virology *81*, 4973-4980.

Betts, M.R., and Harari, A. (2008). Phenotype and function of protective T cell immune responses in HIV. Curr Opin HIV AIDS *3*, 349-355.

Betts, M.R., Nason, M.C., West, S.M., De Rosa, S.C., Migueles, S.A., Abraham, J., Lederman, M.M., Benito, J.M., Goepfert, P.A., Connors, M., *et al.* (2006). HIV nonprogressors preferentially maintain highly functional HIV-specific CD8(+) T cells. Blood *107*, 4781-4789.

Boissonnas, A., Fetler, L., Zeelenberg, I.S., Hugues, S., and Amigorena, S. (2007). In vivo imaging of cytotoxic T cell infiltration and elimination of a solid tumor. Journal of Experimental Medicine *204*, 345-356.

Breart, B., Lemaitre, F., Celli, S., and Bousso, P. (2008). Two-photon imaging of intratumoral CD8(+) T cell cytotoxic activity during adoptive T cell therapy in mice. Journal of Clinical Investigation *118*, 1390-1397.

Castellino, F., Huang, A.Y., Altan-Bonnet, G., Stoll, S., Scheinecker, C., and Germain, R.N. (2006). Chemokines enhance immunity by guiding naive CD8+ T cells to sites of CD4+ T cell-dendritic cell interaction. Nature *440*, 890-895.

Catalfamo, M., Karpova, T., McNally, J., Costes, S.V., Lockett, S.J., Bos, E., Peters, P.J., and Henkart, P.A. (2004). Human CD8(+) T cells store RANTES in a unique secretory compartment and release it rapidly after TcR stimulation. Immunity *20*, 219-230.

Cerottini, J.C., and Brunner, K.T. (1974). Cell-mediated cytotoxicity, allograft rejection, and tumor immunity. Adv Immunol *18*, 67-132.

Chen, H., Piechocka-Trocha, A., Miura, T., Brockman, M.A., Julg, B.D., Baker, B.M., Rothchild, A.C., Block, B.L., Schneidewind, A., Koibuchi, T., *et al.* (2009). Differential neutralization of human immunodeficiency virus (HIV) replication in autologous CD4 T cells by HIV-specific cytotoxic T lymphocytes. J Virol *83*, 3138-3149.

Cocchi, F., DeVico, A.L., Garzino-Demo, A., Arya, S.K., Gallo, R.C., and Lusso, P. (1995). Identification of RANTES, MIP-1 alpha, and MIP-1 beta as the major HIV-suppressive factors produced by CD8+ T cells. Science *270*, 1811-1815.

Cocchi, F., DeVico, A.L., Yarchoan, R., Redfield, R., Cleghorn, F., Blattner, W.A., Garzino-Demo, A., Colombini-Hatch, S., Margolis, D., and Gallo, R.C. (2000). Higher macrophage inflammatory protein (MIP)-1alpha and MIP-1beta levels from CD8+ T cells are associated with asymptomatic HIV-1 infection. Proc Natl Acad Sci U S A *97*, 13812-13817.

Collins, K.L., Chen, B.K., Kalams, S.A., Walker, B.D., and Baltimore, D. (1998). HIV-1 Nef protein protects infected primary cells against killing by cytotoxic T lymphocytes. Nature *391*, 397-401.

Coppieters, K., Amirian, N., and von Herrath, M. (2011). Intravital imaging of CTLs killing islet cells in diabetic mice. J Clin Invest.

Deguine, J., Breart, B., Lemaitre, F., Di Santo, J.P., and Bousso, P. (2010). Intravital Imaging Reveals Distinct Dynamics for Natural Killer and CD8(+) T Cells during Tumor Regression. Immunity *33*, 632-644.

DeVico, A.L., and Gallo, R.C. (2004). Control of HIV-1 infection by soluble factors of the immune response. Nat Rev Microbiol *2*, 401-413.

Dolan, M.J., Kulkarni, H., Camargo, J.F., He, W., Smith, A., Anaya, J.M., Miura, T., Hecht, F.M., Mamtani, M., Pereyra, F., *et al.* (2007). CCL3L1 and CCR5 influence cell-mediated immunity and affect HIV-AIDS pathogenesis via viral entry-independent mechanisms. Nat Immunol *8*, 1324-1336.

Dustin, M.L., Bromley, S.K., Kan, Z.Y., Peterson, D.A., and Unanue, E.R. (1997). Antigen receptor engagement delivers a stop signal to migrating T lymphocytes. P Natl Acad Sci USA *94*, 3909-3913.

Esser, M.T., Krishnamurthy, B., and Braciale, V.L. (1996). Distinct T cell receptor signaling requirements for perforin- or FasL-mediated cytotoxicity. J Exp Med *183*, 1697-1706.

Faroudi, M., Utzny, C., Salio, M., Cerundolo, V., Guiraud, M., Muller, S., and Valitutti, S. (2003). Lytic versus stimulatory synapse in cytotoxic T lymphocyte/target cell interaction: manifestation of a dual activation threshold. Proc Natl Acad Sci U S A *100*, 14145-14150.

Fauce, S.R., Yang, O.O., and Effros, R.B. (2007). Autologous CD4/CD8 co-culture assay: A physiologically-relevant composite measure of CD8(+) T lymphocyte function in HIV-infected persons. Journal of Immunological Methods *327*, 75-81.

Ferbas, J., Giorgi, J.V., Amini, S., Grovit-Ferbas, K., Wiley, D.J., Detels, R., and Plaeger, S. (2000). Antigen-specific production of RANTES, macrophage inflammatory protein (MIP)-1alpha, and MIP-1beta in vitro is a correlate of reduced human immunodeficiency virus burden in vivo. J Infect Dis *182*, 1247-1250.

Fife, B.T., Pauken, K.E., Eagar, T.N., Obu, T., Wu, J., Tang, Q.Z., Azuma, M., Krummel, M.F., and Bluestone, J.A. (2009). Interactions between PD-1 and PD-L1 promote tolerance by blocking the TCR-induced stop signal. Nat Immunol *10*, 1185-U1170.

Freel, S.A., Lamoreaux, L., Chattopadhyay, P.K., Saunders, K., Zarkowsky, D., Overman, R.G., Ochsenbauer, C., Edmonds, T.G., Kappes, J.C., Cunningham, C.K., *et al.* (2010). Phenotypic and Functional Profile of HIV-Inhibitory CD8 T Cells Elicited by Natural Infection and Heterologous Prime/Boost Vaccination. Journal of Virology *84*, 4998-5006.

Friedl, P., and Brocker, E.B. (2004). Reconstructing leukocyte migration in 3D extracellular matrix by time-lapse videomicroscopy and computer-assisted tracking. Methods Mol Biol *239*, 77-90.

Friedman, R.S., Jacobelli, J., and Krummel, M.F. (2006). Surface-bound chemokines capture and prime T cells for synapse formation. Nat Immunol *7*, 1101-1108.

Friedrich, T.C., Valentine, L.E., Yant, L.J., Rakasz, E.G., Piaskowski, S.M., Furlott, J.R., Weisgrau, K.L., Burwitz, B., May, G.E., Leon, E.J., *et al.* (2007). Subdominant CD8+ T-cell responses are involved in durable control of AIDS virus replication. J Virol *81*, 3465-3476.

Genesca, M., Skinner, P.J., Bost, K.M., Lu, D., Wang, Y., Rourke, T.L., Haase, A.T., McChesney, M.B., and Miller, C.J. (2008). Protective attenuated lentivirus immunization induces SIV-specific T cells in the genital tract of rhesus monkeys. Mucosal Immunol *1*, 219-228.

Guidotti, L.G., and Chisari, F.V. (2001). Noncytolytic control of viral infections by the innate and adaptive immune response. Annu Rev Immunol *19*, 65-91.

Gunzer, M., Weishaupt, C., Hillmer, A., Basoglu, Y., Friedl, P., Dittmar, K.E., Kolanus, W., Varga, G., and Grabbe, S. (2004). A spectrum of biophysical interaction modes between T cells and different antigen-presenting cells during priming in 3-D collagen and in vivo. Blood *104*, 2801-2809.

Haase, A.T. (2005). Perils at mucosal front lines for HIV and SIV and their hosts. Nat Rev Immunol *5*, 783-792.

Haase, A.T. (2010). Targeting early infection to prevent HIV-1 mucosal transmission. Nature *464*, 217-223.

Hansen, S.G., Ford, J.C., Lewis, M.S., Ventura, A.B., Hughes, C.M., Coyne-Johnson, L., Whizin, N., Oswald, K., Shoemaker, R., Swanson, T., *et al.* (2011). Profound early control of highly pathogenic SIV by an effector memory T-cell vaccine. Nature *473*, 523-527.

Hansen, S.G., Vieville, C., Whizin, N., Coyne-Johnson, L., Siess, D.C., Drummond, D.D., Legasse, A.W., Axthelm, M.K., Oswald, K., Trubey, C.M., *et al.* (2009). Effector memory T cell responses are associated with protection of rhesus monkeys from mucosal simian immunodeficiency virus challenge. Nat Med *15*, 293-299.

He, J.S., Gong, D.E., and Ostergaard, H.L. (2010). Stored Fas ligand, a mediator of rapid CTL-mediated killing, has a lower threshold for response than degranulation or newly synthesized Fas ligand. J Immunol *184*, 555-563.

Hersperger, A.R., Pereyra, F., Nason, M., Demers, K., Sheth, P., Shin, L.Y., Kovacs, C.M., Rodriguez, B., Sieg, S.F., Teixeira-Johnson, L., *et al.* (2010). Perforin expression directly ex vivo by HIV-specific CD8 T-cells is a correlate of HIV elite control. PLoS Pathog *6*, e1000917.

Hong, J.J., Reynolds, M.R., Mattila, T.L., Hage, A., Watkins, D.I., Miller, C.J., and Skinner, P.J. (2009). Localized populations of CD8 MHC class I tetramer SIV-specific T cells in lymphoid follicles and genital epithelium. PLoS One *4*, e4131.

Hugues, S., Scholer, A., Boissonnas, A., Nussbaum, A., Combadiere, C., Amigorena, S., and Fetler, L. (2007). Dynamic imaging of chemokine-dependent CD8+ T cell help for CD8+ T cell responses. Nat Immunol *8*, 921-930.

Huse, M., Klein, L.O., Girvin, A.T., Faraj, J.M., Li, Q.J., Kuhns, M.S., and Davis, M.M. (2007). Spatial and temporal dynamics of T cell receptor signaling with a photoactivatable agonist. Immunity *27*, 76-88.

Huse, M., Quann, E.J., and Davis, M.M. (2008). Shouts, whispers and the kiss of death: directional secretion in T cells. Nat Immunol *9*, 1105-1111.

Isaaz, S., Baetz, K., Olsen, K., Podack, E., and Griffiths, G.M. (1995). Serial Killing by Cytotoxic T-Lymphocytes - T-Cell Receptor Triggers Degranulation, Re-Filling of the Lytic Granules and Secretion of Lytic Proteins Via a Non-Granule Pathway. European Journal of Immunology *25*, 1071-1079.

Iversen, A.K.N., Stewart-Jones, G., Learn, G.H., Christie, N., Sylvester-Hviid, C., Armitage, A.E., Kaul, R., Beattie, T., Lee, J.K., Li, Y.P., *et al.* (2006). Conflicting selective forces affect T cell receptor contacts in an immunodominant human immunodeficiency virus epitope. Nat Immunol *7*, 179-189.

Janssen, E.M., Lemmens, E.E., Gour, N., Reboulet, R.A., Green, D.R., Schoenberger, S.P., and Pinkoski, M.J. (2010). Distinct roles of cytolytic effector molecules for antigen-restricted killing by CTL in vivo. Immunol Cell Biol *88*, 761-765.

Jenkins, M.R., La Gruta, N.L., Doherty, P.C., Trapani, J.A., Turner, S.J., and Waterhouse, N.J. (2009a). Visualizing CTL activity for different CD8(+) effector T cells supports the idea that lower TCR/epitope avidity may be advantageous for target cell killing. Cell Death Differ *16*, 537-542.

Jenkins, M.R., Tsun, A., Stinchcombe, J.C., and Griffiths, G.M. (2009b). The strength of T cell receptor signal controls the polarization of cytotoxic machinery to the immunological synapse. Immunity *31*, 621-631.

Julg, B., Williams, K.L., Reddy, S., Bishop, K., Qi, Y., Carrington, M., Goulder, P.J., Ndung'u, T., and Walker, B.D. (2010). Enhanced anti-HIV functional activity associated with Gag-specific CD8 T-cell responses. J Virol *84*, 5540-5549.

Kaslow, R.A., Carrington, M., Apple, R., Park, L., Munoz, A., Saah, A.J., Goedert, J.J., Winkler, C., O'Brien, S.J., Rinaldo, C., *et al.* (1996). Influence of combinations of human major histocompatibility complex genes on the course of HIV-1 infection. Nat Med *2*, 405-411.

Kaufman, D.R., Simmons, N.L., and Barouch, D.H. (2009). Mucosal trafficking and differentiation of vaccine-elicited CD8+T-lymphocytes. Retrovirology *6*, -.

Kawakami, N., Nagerl, U.V., Odoardi, F., Bonhoeffer, T., Wekerle, H., and Flugel, A. (2005). Live imaging of effector cell trafficking and autoantigen recognition within the unfolding autoimmune encephalomyelitis lesion. J Exp Med *201*, 1805-1814.

Keefe, D., Shi, L., Feske, S., Massol, R., Navarro, F., Kirchhausen, T., and Lieberman, J. (2005). Perforin triggers a plasma membrane-repair response that facilitates CTL induction of apoptosis. Immunity *23*, 249-262.

Kiepiela, P., Ngumbela, K., Thobakgale, C., Ramduth, D., Honeyborne, I., Moodley, E., Reddy, S., de Pierres, C., Mncube, Z., Mkhwanazi, N., *et al.* (2007). CD8+ T-cell responses to different HIV proteins have discordant associations with viral load. Nat Med *13*, 46-53.

Kojima, Y., Kawasaki-Koyanagi, A., Sueyoshi, N., Kanai, A., Yagita, H., and Okumura, K. (2002). Localization of Fas ligand in cytoplasmic granules of CD8+ cytotoxic T lymphocytes and natural killer cells: participation of Fas ligand in granule exocytosis model of cytotoxicity. Biochem Biophys Res Commun *296*, 328-336.

Kulkarni, H., Agan, B.K., Marconi, V.C., O'Connell, R.J., Camargo, J.F., He, W., Delmar, J., Phelps, K.R., Crawford, G., Clark, R.A., *et al.* (2008). CCL3L1-CCR5 genotype improves the assessment of AIDS Risk in HIV-1-infected individuals. PLoS One *3*, e3165.

Li, Q., Estes, J.D., Schlievert, P.M., Duan, L., Brosnahan, A.J., Southern, P.J., Reilly, C.S., Peterson, M.L., Schultz-Darken, N., Brunner, K.G., *et al.* (2009a). Glycerol monolaurate prevents mucosal SIV transmission. Nature *458*, 1034-1038.

Li, Q., Skinner, P.J., Ha, S.J., Duan, L., Mattila, T.L., Hage, A., White, C., Barber, D.L., O'Mara, L., Southern, P.J., *et al.* (2009b). Visualizing antigen-specific and infected cells in situ predicts outcomes in early viral infection. Science *323*, 1726-1729.

Liu, J.Y., O'Brien, K.L., Lynch, D.M., Simmons, N.L., La Porte, A., Riggs, A.M., Abbink, P., Coffey, R.T., Grandpre, L.E., Seaman, M.S., *et al.* (2009). Immune control of an SIV challenge by a T-cell-based vaccine in rhesus monkeys. Nature *457*, 87-91.

Lowin, B., Hahne, M., Mattmann, C., and Tschopp, J. (1994). Cytolytic T-cell cytotoxicity is mediated through perforin and Fas lytic pathways. Nature *370*, 650-652.

Martz, E. (1976). Multiple Target-Cell Killing by Cytolytic T-Lymphocyte and Mechanism of Cytotoxicity. Transplantation *21*, 5-11.

Matter, A. (1979). Microcinematographic and electron microscopic analysis of target cell lysis induced by cytotoxic T lymphocytes. Immunology *36*, 179-190.

McMichael, A.J., Borrow, P., Tomaras, G.D., Goonetilleke, N., and Haynes, B.F. (2010). The immune response during acute HIV-1 infection: clues for vaccine development. Nat Rev Immunol *10*, 11-23.

Meiraz, A., Garber, O.G., Harari, S., Hassin, D., and Berke, G. (2009). Switch from perforin-expressing to perforin-deficient CD8(+) T cells accounts for two distinct types of effector cytotoxic T lymphocytes in vivo. Immunology *128*, 69-82.

Mellman, I., Coukos, G., and Dranoff, G. (2011). Cancer immunotherapy comes of age. Nature *480*, 480-489.

Mempel, T.R., Pittet, M.J., Khazaie, K., Weninger, W., Weissleder, R., von Boehmer, H., and von Andrian, U.H. (2006). Regulatory T cells reversibly suppress cytotoxic T cell function independent of effector differentiation. Immunity *25*, 129-141.

Migueles, S.A., Laborico, A.C., Shupert, W.L., Sabbaghian, M.S., Rabin, R., Hallahan, C.W., Van Baarle, D., Kostense, S., Miedema, F., McLaughlin, M., *et al.* (2002). HIV-specific CD8(+) T cell proliferation is coupled to perforin expression and is maintained in nonprogressors. Nat Immunol *3*, 1061-1068.

Migueles, S.A., Osborne, C.M., Royce, C., Compton, A.A., Joshi, R.P., Weeks, K.A., Rood, J.E., Berkley, A.M., Sacha, J.B., Cogliano-Shutta, N.A., *et al.* (2008). Lytic Granule Loading of CD8(+) T Cells Is Required for HIV-Infected Cell Elimination Associated with Immune Control. Immunity *29*, 1009-1021.

Miller, M.J., Safrina, O., Parker, I., and Cahalan, M.D. (2004). Imaging the single cell dynamics of CD4+ T cell activation by dendritic cells in lymph nodes. J Exp Med *200*, 847-856.

Miller, M.J., Wei, S.H., Parker, I., and Cahalan, M.D. (2002). Two-photon imaging of lymphocyte motility and antigen response in intact lymph node. Science *296*, 1869-1873.

Molon, B., Gri, G., Bettella, M., Gomez-Mouton, C., Lanzavecchia, A., Martinez, A.C., Manes, S., and Viola, A. (2005). T cell costimulation by chemokine receptors. Nat Immunol *6*, 465-471.

Mora, J.R., and von Andrian, U.H. (2006). T-cell homing specificity and plasticity: new concepts and future challenges. Trends Immunol *27*, 235-243.

Mrass, P., Takano, H., Ng, L.G., Daxini, S., Lasaro, M.O., Iparraguirre, A., Cavanagh, L.L., von Andrian, U.H., Ertl, H.C.J., Haydon, P.G., and Weninger, W. (2006). Random migration precedes stable target cell interactions of tumor-infiltrating T cells. Journal of Experimental Medicine *203*, 2749-2761.

Nobile, C., Rudnicka, D., Hasan, M., Aulner, N., Porrot, F., Machu, C., Renaud, O., Prevost, M.C., Hivroz, C., Schwartz, O., and Sol-Foulon, N. (2010). HIV-1 Nef inhibits ruffles, induces filopodia, and modulates migration of infected lymphocytes. J Virol *84*, 2282-2293.

Poenie, M., Tsien, R.Y., and Schmitt-Verhulst, A.M. (1987). Sequential activation and lethal hit measured by [Ca2+]i in individual cytolytic T cells and targets. EMBO J *6*, 2223-2232.

Porgador, A., Yewdell, J.W., Deng, Y., Bennink, J.R., and Germain, R.N. (1997). Localization, quantitation, and in situ detection of specific peptide-MHC class I complexes using a monoclonal antibody. Immunity *6*, 715-726.

Poropatich, K., and Sullivan, D.J., Jr. (2011). Human immunodeficiency virus type 1 long-term non-progressors: the viral, genetic and immunological basis for disease non-progression. J Gen Virol *92*, 247-268.

Purbhoo, M.A., Boulter, J.M., Price, D.A., Vuidepot, A.L., Hourigan, C.S., Dunbar, P.R., Olson, K., Dawson, S.J., Phillips, R.E., Jakobsen, B.K., *et al.* (2001). The human CD8

coreceptor effects cytotoxic T cell activation and antigen sensitivity primarily by mediating complete phosphorylation of the T cell receptor zeta chain. Journal of Biological Chemistry *276*, 32786-32792.

Purbhoo, M.A., Irvine, D.J., Huppa, J.B., and Davis, M.M. (2004). T cell killing does not require the formation of a stable mature immunological synapse. Nat Immunol *5*, 524-530.

Reynolds, M.R., Rakasz, E., Skinner, P.J., White, C., Abel, K., Ma, Z.M., Compton, L., Napoe, G., Wilson, N., Miller, C.J., *et al.* (2005). CD8+ T-lymphocyte response to major immunodominant epitopes after vaginal exposure to simian immunodeficiency virus: too late and too little. J Virol *79*, 9228-9235.

Rothstein, T.L., Mage, M., Jones, G., and McHugh, L.L. (1978). Cytotoxic T lymphocyte sequential killing of immobilized allogeneic tumor target cells measured by time-lapse microcinematography. J Immunol *121*, 1652-1656.

Saez-Cirion, A., Lacabaratz, C., Lambotte, O., Versmisse, P., Urrutia, A., Boufassa, F., Barre-Sinoussi, F., Delfraissy, J.F., Sinet, M., Pancino, G., *et al.* (2007). HIV controllers exhibit potent CD8 T cell capacity to suppress HIV infection ex vivo and peculiar cytotoxic T lymphocyte activation phenotype. P Natl Acad Sci USA *104*, 6776-6781.

Saez-Cirion, A., Shin, S.Y., Versmisse, P., Barre-Sinoussi, F., and Pancino, G. (2010). Ex vivo T cell-based HIV suppression assay to evaluate HIV-specific CD8+ T-cell responses. Nat Protoc *5*, 1033-1041.

Scarlatti, G., Tresoldi, E., Bjorndal, A., Fredriksson, R., Colognesi, C., Deng, H.K., Malnati, M.S., Plebani, A., Siccardi, A.G., Littman, D.R., *et al.* (1997). In vivo evolution of HIV-1 co-receptor usage and sensitivity to chemokine-mediated suppression. Nat Med *3*, 1259-1265.

Schmitz, J.E., Johnson, R.P., McClure, H.M., Manson, K.H., Wyand, M.S., Kuroda, M.J., Lifton, M.A., Khunkhun, R.S., McEvers, K.J., Gillis, J., *et al.* (2005). Effect of CD8+ lymphocyte depletion on virus containment after simian immunodeficiency virus SIVmac251 challenge of live attenuated SIVmac239delta3-vaccinated rhesus macaques. J Virol *79*, 8131-8141.

Schmitz, J.E., Kuroda, M.J., Santra, S., Sasseville, V.G., Simon, M.A., Lifton, M.A., Racz, P., Tenner-Racz, K., Dalesandro, M., Scallon, B.J., *et al.* (1999). Control of viremia in simian immunodeficiency virus infection by CD8+ lymphocytes. Science *283*, 857-860.

Schneider, H., Downey, J., Smith, A., Zinselmeyer, B.H., Rush, C., Brewer, J.M., Wei, B., Hogg, N., Garside, P., and Rudd, C.E. (2006). Reversal of the TCR stop signal by CTLA-4. Science *313*, 1972-1975.

Schwartz, O., Marechal, V., Le Gall, S., Lemonnier, F., and Heard, J.M. (1996). Endocytosis of major histocompatibility complex class I molecules is induced by the HIV-1 Nef protein. Nat Med *2*, 338-342.

Shanker, A., Brooks, A.D., Jacobsen, K.M., Wine, J.W., Wiltrout, R.H., Yagita, H., and Sayers, T.J. (2009). Antigen presented by tumors in vivo determines the nature of CD8+ T-cell cytotoxicity. Cancer Res *69*, 6615-6623.

Simmons, G., Reeves, J.D., Hibbitts, S., Stine, J.T., Gray, P.W., Proudfoot, A.E.I., and Clapham, P.R. (2000). Co-receptor use by HIV and inhibition of HIV infection by chemokine receptor ligands. Immunol. Rev. *177*, 112-126.

Stinchcombe, J.C., Bossi, G., Booth, S., and Griffiths, G.M. (2001). The immunological synapse of CTL contains a secretory domain and membrane bridges. Immunity *15*, 751-761.

Stoll, S., Delon, J., Brotz, T.M., and Germain, R.N. (2002). Dynamic imaging of T cell-dendritic cell interactions in lymph nodes. Science *296*, 1873-1876.

Thiery, J., Keefe, D., Boulant, S., Boucrot, E., Walch, M., Martinvalet, D., Goping, I.S., Bleackley, R.C., Kirchhausen, T., and Lieberman, J. (2011). Perforin pores in the endosomal membrane trigger the release of endocytosed granzyme B into the cytosol of target cells. Nat Immunol *12*, 770-777.

Tjernlund, A., Zhu, J., Laing, K., Diem, K., McDonald, D., Vazquez, J., Cao, J., Ohlen, C., McElrath, M.J., Picker, L.J., and Corey, L. (2010). In situ detection of Gag-specific CD8+ cells in the GI tract of SIV infected Rhesus macaques. Retrovirology *7*, 12.

Uchida, T. (2011). Development of a cytotoxic T-lymphocyte-based, broadly protective influenza vaccine. Microbiol Immunol *55*, 19-27.

Valitutti, S., Coombs, D., and Dupre, L. (2010). The space and time frames of T cell activation at the immunological synapse. FEBS Lett *584*, 4851-4857.

Valitutti, S., Muller, S., Dessing, M., and Lanzavecchia, A. (1996). Different responses are elicited in cytotoxic T lymphocytes by different levels of T cell receptor occupancy. J Exp Med *183*, 1917-1921.

Wagner, L., Yang, O.O., Garcia-Zepeda, E.A., Ge, Y.M., Kalams, S.A., Walker, B.D., Pasternack, M.S., and Luster, A.D. (1998). beta-chemokines are released from HIV-1-specific cytolytic T-cell granules complexed to proteoglycans. Nature *391*, 908-911.

Waterhouse, N.J., Sutton, V.R., Sedelies, K.A., Ciccone, A., Jenkins, M., Turner, S.J., Bird, P.I., and Trapani, J.A. (2006). Cytotoxic T lymphocyte-induced killing in the absence of granzymes A and B is unique and distinct from both apoptosis and perforin-dependent lysis. J Cell Biol *173*, 133-144.

Weigelin, B., and Friedl, P. (2010). A three-dimensional organotypic assay to measure target cell killing by cytotoxic T lymphocytes. Biochem Pharmacol *80*, 2087-2091.

Weninger, W., Manjunath, N., and von Andrian, U.H. (2002). Migration and differentiation of CD8+ T cells. Immunol Rev *186*, 221-233.

Wiedemann, A., Depoil, D., Faroudi, M., and Valitutti, S. (2006). Cytotoxic T lymphocytes kill multiple targets simultaneously via spatiotemporal uncoupling of lytic and stimulatory synapses. P Natl Acad Sci USA *103*, 10985-10990.

Wolf, K., Muller, R., Borgmann, S., Brocker, E.B., and Friedl, P. (2003). Amoeboid shape change and contact guidance: T-lymphocyte crawling through fibrillar collagen is independent of matrix remodeling by MMPs and other proteases. Blood *102*, 3262-3269.

Yang, O.O., Kalams, S.A., Trocha, A., Cao, H.Y., Luster, A., Johnson, R.P., and Walker, B.D. (1997). Suppression of human immunodeficiency virus type 1 replication by CD8(+) cells: Evidence for HLA class I-restricted triggering of cytolytic and noncytolytic mechanisms. Journal of Virology *71*, 3120-3128.

Yang, O.O., Sarkis, P.T.N., Trocha, A., Kalams, S.A., Johnson, R.P., and Walker, B.D. (2003). Impacts of avidity and specificity on the antiviral efficiency of HIV-1-specific CTL. Journal of Immunology *171*, 3718-3724.

Zagury, D., Bernard, J., Thierness, N., Feldman, M., and Berke, G. (1975). Isolation and Characterization of Individual Functionally Reactive Cytotoxic T-Lymphocytes - Conjugation, Killing and Recycling at Single Cell Level. European Journal of Immunology *5*, 818-822.

Zhang, Z., Schuler, T., Zupancic, M., Wietgrefe, S., Staskus, K.A., Reimann, K.A., Reinhart, T.A., Rogan, M., Cavert, W., Miller, C.J., *et al.* (1999). Sexual transmission and propagation of SIV and HIV in resting and activated CD4+ T cells. Science *286*, 1353-1357.

Zuccato, E., Blott, E.J., Holt, O., Sigismund, S., Shaw, M., Bossi, G., and Griffiths, G.M. (2007). Sorting of Fas ligand to secretory lysosomes is regulated by mono-ubiquitylation and phosphorylation. J Cell Sci *120*, 191-199.